Journal of South American Earth Sciences xxx (2009) xxx–xxx

Contents lists available at ScienceDirect

Journal of South American Earth Sciences

journal homepage: www.elsevier.com/locate/jsames

Geology and petrology of a deep crustal zone from the Famatinian paleo-arc, Sierras de Valle Fértil and La Huerta, San Juan, Argentina

J.E. Otamendi [a,e,*], G.I. Vujovich [b,e], J.D. de la Rosa [c], A.M. Tibaldi [a,e], A. Castro [c], R.D. Martino [d,e], L.P. Pinotti [a,e]

[a] Departamento de Geología, Universidad Nacional de Río Cuarto, X5804BYA Río Cuarto, Córdoba, Argentina
[b] Departamento de Ciencias Geológicas, Universidad de Buenos Aires, Facultad de Ciencias Exactas y Naturales, 1428 Buenos Aires, Argentina
[c] Departamento de Geología, Universidad de Huelva, E21071 Huelva, Spain
[d] Departamento de Geología, Universidad de Nacional de Córdoba, Facultad de Ciencias Exactas y Naturales, Argentina
[e] Consejo Nacional de Investigaciones Científicas y Técnicas, Argentina

ARTICLE INFO

Article history:
Received 16 December 2007
Accepted 11 November 2008
Available online xxxx

Keywords:
Magmatic arc
Famatinian
Gabbro
Diorite
Tonalite
Granodiorite

ABSTRACT

The ranges of the Sierras Valle Fértil-La Huerta expose natural cross sections through a paleo-arc crust that formed in the Late Cambrian - Early Ordovician Famatinian magmatic arc, northwestern Argentina. Thick mafic sequences of amphibole gabbronorites to orthopyroxene-amphibole-biotite diorites form the lower levels of the exposed paleo-arc section. This mafic unit includes lens-shaped bodies of olivine-bearing cumulate rocks and tabular-shaped sill/dike intrusions of fine-grained chilled amphibole gabbro. The mafic magmas were emplaced into regional metasedimentary sequences at lower crustal levels, corresponding to pressure from 5 to 7 kbar. Gabbronorites likely representing the parental magmas that fluxed into the exposed paleo-arc crust differ from primitive magmatic arc rocks in having somewhat lower Mg-number (*ca.* 0.60) and compatible (Cr and Ni) trace element contents, and slightly higher Al_2O_3 contents. This difference is taken to indicate that a pyroxene-rich olivine-bearing assemblage with a bulk high Mg/Fe ratio and low Al_2O_3 content crystallized from mantle-derived melts before mafic magmas reached the crustal levels currently exhumed. However, some gabbronorites have incompatible trace element signatures typical of primitive mafic arc magmatism. Igneous rocks to some extent more evolved than those of the mafic unit make up a tonalite-dominated intermediate unit. The intermediate unit consists of a heterogeneous suite that ranges from orthopyroxene-bearing amphibole-rich diorites to biotite-rich amphibole-poor tonalites. Within the intermediate unit, chilled mafic rocks are found as a network of dikes, whereas metasedimentary migmatites appear interlayered as m-wide septa and km-long strips. The tonalite-dominated intermediate unit passes into a granodiorite batholith through a transitional zone that is up to 2-km wide. The boundary zone separating the tonalite-dominated and granodiorite-dominated units is characterized by mingling of tonalitic and leucogranitic magmas, which together appear multiply-intruded by mafic sill/dike bodies. Within the tonalite- and granodiorite-dominated units, the less evolved mafic rocks occur as: (1) bodies tens of meters long, (2) chilled dikes and sills, and (3) microgranular inclusions (enclaves), supporting the inference that mafic magmatism was the main source for generating a vast volume of intermediate and silicic igneous rocks. Mass balance calculations and trace element systematics are combined to demonstrate that tonalites and granodiorites formed by concurrent closed-system fractional crystallization and open-system incorporation of paragneissic migmatites and/or anatectic leucogranites into the evolving igneous sequence. This study argues that the sequence of igneous rocks from Valle Fértil-La Huerta was formed as the result of complementary petrogenetic processes that operated concurrently at different levels of the Famatinian arc crust.

1. Introduction

The results of plate tectonic theory revealed an obvious spatial relation between the basalt-andesite-dacite-rhyolite magmatic suites and destructive plate margins (see Wilson, 1989). Since then, subduction-related magmatism has been the central issue of research aimed at deciphering the physical and chemical processes involved in magmatic evolution. The issue encompasses understanding natural processes that occur from the subducting slab and mantle sources to the plumbing system of volcanic edifices. Our understanding of each petrogenetic stage involved in the generation of subduction-related magmatism is in direct function with the depth within the Earth where a petrologic process

* Corresponding author. Address: Departamento de Geología, Universidad Nacional de Río Cuarto, X5804BYA Río Cuarto, Cordoba, Argentina. Tel.: +54 358 4676198; fax: +54 358 4680280.
E-mail address: jotamendi@exa.unrc.edu.ar (J.E. Otamendi).

0895-9811/$ - see front matter © 2008 Elsevier Ltd. All rights reserved.
doi:10.1016/j.jsames.2008.11.007

takes place. Active volcanoes in island and continental magmatic arcs allow integrating the stratigraphic succession with petrologic modeling; several studies following this approach have been able to demonstrate what mechanisms operate to create petrologic diversity from the deepest crustal roots to magma chambers residing beneath active volcanic fields (Feeley et al., 1996; Gamble et al., 1999; Dungan et al., 2001; among others). The success of these studies in unraveling petrologic processes is undeniable, but some uncertainty with respect to the conclusion will remain until the petrologic mechanisms, which are largely inferred from chemical and isotopic data, may be proved through field relations. For this reason, the few natural examples exposing low levels of paleo-arc crustal sections are being intensely studied (see DeBari and Coleman, 1989; DeBari, 1994; Ducea et al., 2003; Kepleis et al., 2004; Greene et al., 2006; Garrido et al., 2006). Following this line of research, this study introduces the geology and petrology of the deep seated levels of the Famatinian magmatic arc.

The Famatinian magmatic arc in western Argentina is a differentially exhumed section of an Upper-Cambrian to Early-Ordovician arc that formed during plate subduction beneath a Gondwanan margin. Owing to present-day Andean tectonic forces, the Famatinian arc is seen for more than 1500 km along strike, even though few isolated exposures of Famatinian plutonic rock are found south of 33°S, the transition from plutonic to volcanic Famatinian rocks can be followed over large regions in northwestern Argentina (Rapela et al., 1992; Toselli et al., 1996; Pankhurst et al., 1998, 2000; Coira et al., 1999; Sato et al., 2003; Lucassen and Franz, 2005). The deepest seated levels of the Famatinian magmatic arc are exposed along Sierras Valle Fértil-La Huerta (Vujovich et al., 1996; Murra and Baldo, 2006; Otamendi et al., 2008). In this study, we use field relationships, mineral chemistry, major-element and trace-element whole rock geochemistry with the aim of: (1) addressing the stratigraphic constitution of the Sierras Valle Fértil-La Huerta showing that the sequence previously mapped as an entirely metamorphosed package is a belt of plutonic rocks assembled by arc-related magmatism; and (2) deciphering the petrologic mechanisms responsible for generating a magmatic sequence encompassing from mafic to silicic igneous rocks and showing progression of more silicic rocks towards upper paleocrustal levels.

2. Geological setting: Famatinian magmatic arc

The Famatinian belt of central Argentina is a subduction-related magmatic arc that was active from the most Upper Cambrian to the Middle Ordovician (Rapela et al., 1992; Toselli et al., 1996; Pankhurst et al., 1998, 2000; Sato et al., 2003; Lucassen and Franz, 2005). Magmatic activity in the central section of the arc ended when an allochthonous terrane collided against the Gondwana margin (Ramos et al., 1996; Thomas and Astini, 1996). The deepest plutonic levels of the arc are currently exposed as a roughly N–S striking wide belt extending for about 600 km between 28° and 33°S (Fig. 1). Between 22° and 28°S, Ordovician eruptive igneous rocks appear interbedded with sedimentary rocks in the Puna – Altiplano region (Turner and Méndez, 1979; Coira et al., 1999; Viramonte et al., 2007) and in the Sistema de Famatina (de Alba, 1979; Toselli et al., 1990; Mannhein and Miller, 1996; Cisterna, 2001; Fanning et al., 2004; Astini and Dávila, 2004). The stratigraphy of the Famatinian arc varies along strike as it was affected by several major tectonic cycles. The central section was closed by a continent-continent collision, and as a whole was variably rifted during the Mesozoic. In spite of having been fragmented in separated fault-bounded blocks, the current locations of the fore-arc, main-arc and back-arc of the Famatinian arc have been successfully deciphered (Saavedra et al., 1998; Pankhurst et al., 2000; Astini and Dávila, 2004; Büttner et al., 2005). According to Quenardelle and Ramos (1999) the central section (i.e. 28°–33°S) of the

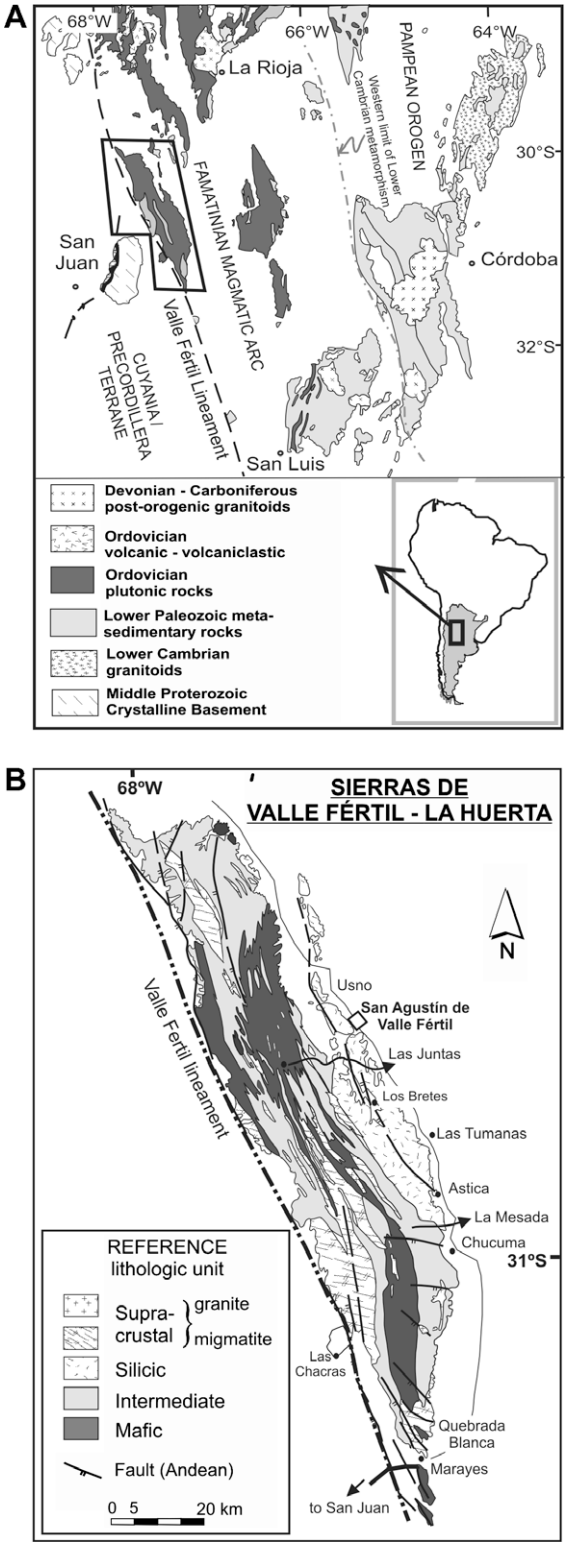

Fig. 1. (A) Map showing the location of the study area with respect to the Pampean orogen, Famatinian magmatic arc and Cuyania and/or Precordillera terrane. This map was modified after Vujovich and Ramos (1999) by using geological information discussed in text. Inset shows the location of the Famatinian arc in Argentina. The study area is outlined within the map. (B) Simplified geologic map of the Sierras de Valle Fértil-La Huerta taken after the geological maps of Mirré (1976) and Vujovich et al. (1996, 1998). This also shows the location of the areas where were obtained the data and samples studied here.

Please cite this article in press as: Otamendi, J.E. et al., Geology and petrology of a deep crustal zone from the Famatinian paleo-arc, Sierras ..., J. S. Am. Earth Sci. (2009), doi:10.1016/j.jsames.2008.11.007

Famatinian arc can be divided into an outboard Famatina terrane being to the west, and an eastern "interior" arc intruded into the Pampia terrane (see Ramos, 1995; Pankhurst et al., 1998). As seen in other examples of exposed plutonic regional-scale Cordilleran-type batholiths, the Famatinian belt includes an I-type dominated plutonic belt along side of an S-type dominated belt (see Toselli et al., 1996; Pankhurst et al., 2000; Rossi et al., 2002). Within the Sierras de Famatina, Los Llanos-Chepes-Ulapes, and Valle Fértil-La Huerta, the most abundant igneous rocks making up regional-scale batholiths are calc-alkaline metaluminous I-type granitoids, whereas weakly or strongly peraluminous felsic granitoids appear in lesser amounts but are widespread (Toselli et al., 1996; Saavedra et al., 1998; Pankhurst et al., 2000). Exactly the opposite occurs in other sierras among which Fiambalá, Capillita, Zapata, and in part Velasco are outstanding examples (Toselli et al., 1996; Rossi et al., 2002). A feature of the Famatinian arc is that every plutonic batholith intrudes supracrustal sedimentary packages largely consisting of siliciclastic sediments with subordinate interlayered carbonate beds (Caminos, 1979). Irrespective of having been metamorphosed under contact aureole or regional dynamothermally Barrovian-type regimes, the supracrustal sequences experienced metamorphism broadly synchronous with plutonic activity (Pankhurst et al., 2000; and references therein). Given that progressively upper levels of the Famatinian arc are exposed northward along strike, the non- to weakly-metamorphosed sedimentary units in the Puna and northern Sierras Pampeanas were extended to the south (Aceñolaza et al., 2000). Thus, the Late Neoproterozoic - Early Cambrian thick turbiditic packages and the Late Cambrian shallow marine sediments are the most likely protoliths to the metamorphic units hosting the deep-seated Famatinian plutonic rocks, whereas epizonal plutons in the Sistema de Famatina and neighbouring areas intruded into early Ordovician volcano-sedimentary sequences formed during an early magmatic arc stage (Toselli et al., 1996; Cisterna, 2001; Astini and Dávila, 2004; and references therein).

3. Local geological features from the Sierras Valle Fértil-La Huerta

Within the western belt of the currently exposed Famatinian magmatic arc, the Sierras Valle Fértil-La Huerta contain fairly well-exposed sections showing the transition between lower-crustal and upper-crustal levels (Otamendi et al., 2008). The reconstruction of the Famatinian arc suggests that this deep seated crustal sequence formed in an outboard belt (e.g. Quenardelle and Ramos, 1999). Tilting and uplifting of the studied crustal section during emplacement in the upper crust might be primarily related to the collision between a Laurentia-derived terrane and the proto-Pacific margin of Gondwana (Thomas and Astini, 1996; Ramos et al., 1996). The strongest evidence for the existence of two distinct continental landmasses is the existence of a paleo-suture called the Valle Fértil lineament along the western border of the Sierras Valle Fértil and La Huerta (Giménez et al., 2000; and Fig. 1). The best age recorded by high-strained metaigneous rocks showed that a late-collisonal exhumation stage was still active during the Early Silurian (e.g. Castro de Machuca et al., 2008). Triassic basalts associated with intra-crustal rifting overlie Ordovician granodiorites (Mirré, 1976) indicating that the low crust of the Famatinian arc was exposed and eroded by that time. The Sierra de Valle Fértil-La Huerta is a fault-bounded crystalline block (140-km-long and up to 30-km-wide) uplifted by a major Andean W-verging reverse fault (Jordan and Allmendinger, 1986).

Field and petrologic studies establish the position of rock units at the time the magmatism was active (Mirré, 1976; Vujovich et al., 1996, 1998). In this reconstruction, the upper part of the exposed section corresponds to its eastern boundary, whereas deeper levels of Ordovician crust are exposed to the west. From west to east, the lithologic units display a progression towards more evolved igneous compositions. In general, the stratigraphy may be described considering four units: (1) a complex layered mafic unit containing mafic/ultramafic olivine-bearing cumulates. The mafic unit is dominated by amphibole gabbronorites and diorites enclosing a suite of chilled mafic sills, dikes and enclaves. (2) An intermediate unit comprising an extremely heterogeneous suite of amphibole- and biotite-rich tonalites. This tonalitic-dominated unit is sometimes separated from the mafic unit by a migmatite-dominated belt. (3) The uppermost igneous unit is a batholith-scale granodiorite, which hosts chilled mafic dikes and enclaves, includes bodies of amphibole-bearing gabbros, has late-magmatic felsic dikes, and in places passes into monzogranite. (4) A supracrustal metasedimentary unit dominated by paragneissic migmatites (metatexite >> diatexite) that occur as km-long strips interlayered with igneous mafic and intermediate rocks or as widespread septa enclosed by gabbronorites and tonalites. The metamorphic supracrustal unit also contains marble/calcsilicate beds that locally appear as km-scale belts within igneous rocks. Garnet-bearing leucogranites, which were derived after partial melting of pelitic-migmatites, are widespread through the sierra as tabular sills or lensoidal bodies. Metapelitic and semipelitic migmatites interlayered in the mafic unit record peak metamorphic pressures between 5.2 and 7.1 kbar at granulite-facies temperatures (Otamendi et al., 2008).

The timing of magmatism in the Sierras Valle Fértil-La Huerta is fairly well-constrained by published geochronology ages (Pontoriero and Castro de Machuca, 1999; Pankhurst et al., 1998, 2000; Roeske et al., 2005). These data suggest that magmatism was active during around 40 Ma (500–460 Ma); however, at least in the Valle Fértil section, the chief magmatic addition occurred between 490 and 468 Ma (Stair et al., 2007).

4. Rock units and petrography

Four localities were chosen for this study: (1) the field relations among gabbro/diorite, migmatites and tonalite were observed to the west, north, and around Las Juntas (Fig. 1B). (2) The transitional boundary from the tonalite-dominated sequence to the granodiorite was mapped along the La Mesada valley (GVF14 to 17, labels correspond to samples presented in Table 1). (3) Typical granodiorites were taken a few kilometers to east of Los Bretes (GVF12 – GVF30-31), while other granodiorites were obtained in the Las Tumanas (GVF10-11) close to the granodioritic sample dated by Pankhurst et al. (2000). (4) The complex interlayering between metatexite- to diatexite-migmatites and igneous lithologic types was investigated at Quebrada Blanca (Fig. 1B). After mapping and characterizing through petrographic analysis and whole-rock chemistry the type of rock, the lithologic units were named according to the most abundant rock type. These units should not be taken as formally-defined stratigraphic units. An obvious first-order distinction is that there are igneous plutonic and metasedimentary units. Since each igneous unit is made up of several rock types, these units are characterized using major-element geochemical groups that better define the range of lithologic types.

4.1. Mafic igneous rock unit

We have characterized this unit through observations around Las Juntas (Fig. 1B). The regional distribution is based on early mapping (e.g. Mirré, 1976; Vujovich et al., 1996, 1998). The majority of the mafic rocks show mineral composition, textural relations and structural features developed under both primary igneous and sub-solidus conditions. However, there also exist mafic rocks

Please cite this article in press as: Otamendi, J.E. et al., Geology and petrology of a deep crustal zone from the Famatinian paleo-arc, Sierras ..., J. S. Am. Earth Sci. (2009), doi:10.1016/j.jsames.2008.11.007

Table 1A
Whole-rock major element and modal analyses of rock from Sierras La Huerta-Valle Fértil.

Sample	Mafic unit											
	LHBL1	LHBL5	LHBL6 inc/LHBL5	LHBL20	LHBL22	LHBL23	LHBL25 leucoDio	VFJA7 cumulate	VFCA1A	VFCA1B sill	VFCA4A sill	VFCA4B
SiO_2	52.56	62.20	44.59	46.63	47.73	53.25	70.51	42.03	46.76	43.36	45.22	64.57
TiO_2	0.77	0.81	1.20	0.46	0.94	0.61	0.73	0.15	1.11	1.12	0.93	0.76
Al_2O_3	18.08	16.06	17.81	15.82	14.73	19.39	11.54	19.16	20.45	18.04	17.94	15.41
$Fe_2O_3^*$	10.15	7.31	14.13	9.91	13.11	5.71	6.52	9.41	12.70	14.51	13.26	6.71
MnO	0.15	0.14	0.29	0.16	0.24	0.10	0.07	0.13	0.23	0.23	0.22	0.13
MgO	3.73	2.50	7.82	14.34	8.86	4.05	2.44	16.80	5.61	8.29	7.89	2.48
CaO	9.31	6.31	11.72	9.82	12.71	8.77	3.14	10.73	9.53	11.54	11.92	5.82
Na_2O	1.83	2.33	1.15	0.85	1.08	2.80	2.02	0.53	2.37	1.64	1.51	2.54
K_2O	0.99	0.96	0.34	0.73	0.17	0.91	1.12	0.07	0.41	0.43	0.33	0.46
P_2O_5	0.11	0.29	0.27	0.05	0.08	0.61	0.02	0.02	0.28	0.10	0.14	0.09
LOI	1.83	1.04	0.60	1.25	0.40	3.06	1.69	1.18	0.53	0.88	0.89	0.73
Total	99.51	99.95	99.92	100.02	100.05	99.26	99.80	100.21	99.98	100.14	100.25	99.70
Mg#	0.40	0.38	0.50	0.72	0.55	0.56	0.40	0.76	0.44	0.50	0.51	0.40
	LHBL1	LHBL5	LHBL6	LHBL20	LHBL22			VFJA7	VFCA1A	VFCA1B	VFCA4A	VFCA4B
Modal crysts (vol.%)												
Qtz	16	34										33
Pl	46	44	44	34	49			21	57	38	43	53
Bt	12	12							2	2	1	3
Amph	7		29	35	6			44	36	52	51	7
Opx		3	13	30	13			15				<1
Cpx	5		6		27			4				
Mt	3	4	4	2	4			1		6	4	3
Sec	11	3	4		1			<1	5	1	1	1
Ap	tr	tr	<1		<1					tr	<1	<1
Zrn		tr										tr
Ol								6				
Spl								9				

Sample	Mafic unit										
	VFO1A	VFO1B inc/VFO1A	VFO3	VFO4A sill	VFO4B	VFO6	VFO7	VFO8	VFO9	VFO10B	VFO12
SiO_2	54.52	45.56	45.26	42.55	47.98	52.16	42.10	45.87	46.37	61.25	59.37
TiO_2	0.93	0.88	0.16	1.11	1.30	1.18	1.49	0.89	1.27	0.83	0.89
Al_2O_3	17.85	15.92	28.34	16.96	19.11	18.20	17.56	16.23	16.13	15.47	17.44
$Fe_2O_3^*$	9.38	12.40	3.46	15.74	12.93	11.48	17.22	13.99	15.04	8.32	7.05
MnO	0.15	0.28	0.06	0.24	0.23	0.20	0.28	0.28	0.26	0.13	0.13
MgO	4.26	8.95	3.85	8.56	4.78	4.29	6.89	9.71	7.19	2.24	2.07
CaO	7.75	10.74	16.99	11.91	9.78	8.83	12.30	11.06	11.02	9.99	8.02
Na_2O	2.29	1.65	0.78	1.26	2.16	2.19	1.05	1.28	1.41	0.95	2.77
K_2O	1.76	1.22	0.11	0.35	0.35	0.53	0.20	0.22	0.24	0.07	0.26
$P2O_5$	0.21	0.16	0.02	0.04	0.30	0.26	0.26	0.12	0.19	0.23	0.25
LOI	0.92	1.38	0.80	1.01	0.17	0.29	0.57	0.49	0.48	0.22	0.98
Total	100.02	99.14	99.83	99.73	99.09	99.61	99.92	100.14	99.60	99.70	99.23
Mg#	0.45	0.56	0.66	0.49	0.40	0.40	0.42	0.55	0.46	0.32	0.34
	VFO1A	VFO1B	VFO3	VFO4A	VFO4B	VFO6	VFO7	VFO8	VFO9	VFO10B	
Modal crysts (vol.%)											
Qtz	22	1			9	8			5	25	
Pl	41	26	79	35	57	61	38	36	39	50	
Bt	14	7			2	2					
Amph	19	63	19	60	18	15	48	49	46	5	
Opx					9	8	1	11	2		
Cpx			1	tr				2	1	16	
Mt	2	2	<1	5	5	5	11	2	4	3	
Sec	1	2	1	<1	1	<1	2	1	2	<1	
Ap	1	<1	<1	<1	<1	1	1	<1	1	<1	
Zrn	tr	tr	tr			<1	<1		tr	<1	

Sample	Intermediate tonalitic unit				Silicic granodioritic unit				
	GVF14	GVF15 inc/GVF14	GVF16	GVF17	GVF10	GVF11 inc/GVF10	GVF12	GVF30	GVF31 inc/GVF30
SiO_2	61.44	52.49	63.20	66.33	63.82	59.20	67.00	62.67	56.75
TiO_2	0.76	1.21	0.81	0.70	0.70	1.02	0.56	0.71	1.06
Al_2O_3	16.85	17.30	16.24	15.40	15.84	16.40	14.94	16.51	16.43
$Fe_2O_3^*$	6.78	11.22	6.50	5.34	5.84	7.98	4.85	7.09	10.49
MnO	0.13	0.21	0.11	0.09	0.12	0.16	0.13	0.15	0.13
MgO	2.24	3.62	2.15	1.57	1.83	2.56	1.41	2.04	3.58
CaO	6.05	8.28	5.55	5.13	5.16	5.79	4.08	5.63	6.75
Na_2O	2.94	2.64	2.76	2.92	2.92	2.99	3.15	3.24	2.94
K_2O	1.75	1.80	1.71	1.68	2.17	2.11	2.62	2.23	2.02
P_2O_5	0.23	0.32	0.19	0.17	0.19	0.32	0.15	0.19	0.26
LOI	0.84	0.63	0.68	0.62	1.11	0.8	0.46	0.20	0.27
Total	100.01	99.72	99.90	99.95	99.70	99.33	99.35	100.66	100.68
Mg#	0.37	0.37	0.37	0.34	0.36	0.36	0.34	0.34	0.38

Please cite this article in press as: Otamendi, J.E. et al., Geology and petrology of a deep crustal zone from the Famatinian paleo-arc, Sierras ..., J. S. Am. Earth Sci. (2009), doi:10.1016/j.jsames.2008.11.007

Table 1A (*continued*)

Sample	Intermediate tonalitic unit				Silicic granodioritic unit				
	GVF14	GVF15	GVF16	GVF17	GVF10	GVF11	GVF12	GVF30	GVF31
Modal crysts (vol.%)									
Qtz	32	13	34	37	24	22	35	28	18
Pl	41	39	36	36	44	43	33	41	47
Kfs					9		12		
Bt	14	13	15	14	13	22	10	16	16
Amph	10	31	13	9	6	7	4	10	14
Mt	1	1	1	1	1	1	1	1	1
Ep	<1	1	<1	1	1	2	3	2	2
Sec	1	1	1	1	1	1	<1	1	<1
Ap	<1	1	<1	1	tr	1	<1	tr	1
Zrn	tr	tr	tr	tr	tr	tr	tr	tr	tr
Sph	tr	<1	<1	<1	tr	<1	<1	tr	tr
Aln	<1						<1		

Sample	Supracrustal metasedimentary rocks and anatectic leucogranites							
	LHBL41 migma	LHBL43 migma	LHBL44 migma	VFO2A migma	VFO11 migma	VFO2C leucogran	LHBL26 leucogran	LHLB46 leucosom
SiO_2	74.46	62.34	70.69	56.48	63.80	73.67	73.48	78.59
TiO_2	0.76	1.26	1.07	1.15	1.23	0.11	0.14	0.12
Al_2O_3	9.89	16.67	11.88	19.71	15.69	14.68	13.56	11.56
$Fe_2O_3^*$	5.63	8.13	6.19	10.09	8.61	0.52	1.96	1.06
MnO	0.09	0.12	0.08	0.19	0.22	0.01	0.04	0.02
MgO	2.42	3.64	2.38	4.36	3.27	0.27	0.84	0.55
CaO	1.92	1.37	1.36	0.69	1.37	1.36	1.38	1.89
Na_2O	1.63	1.57	1.77	1.16	2.08	2.83	2.11	2.23
K_2O	1.42	2.65	1.84	4.40	2.54	5.74	4.61	3.16
P_2O_5	0.07	0.07	0.07	0.08	0.08	0.10	0.05	0.06
LOI	1.16	1.34	2.14	1.11	1.14	0.73	1.16	0.82
Total	99.45	99.16	99.47	99.42	100.03	100.02	99.33	100.06
Mg#	0.43	0.44	0.41	0.44	0.40	0.48	0.43	0.48

Major oxides in weight%. Total Fe reported as $Fe_2O_3^*$. For this reason Mg# is MgO/(MgO + FeO) on molar basis but after converting $Fe_2O_3^*$ to FeO^*. Modal proportion was determined by point counting (1200–2000 points); <1 is modal proportion between 0.1% and 1%, whereas tr is lower than 0.1%. Inc/LHBL5 indicates that the sample is a microgranular inclusion in sample LHBL5.

showing either pristine igneous features or a well-developed metamorphic fabric (Fig. 2A–C). The latter are mafic migmatites in which the primary features were completely overprinted (Fig. 2D), the former are gabbroic layered and cumulate rocks. The most abundant rock is an amphibole-rich gabbronorite constituted by plagioclase, amphibole, orthopyroxene, oxides, apatite and zircon, occasionally bearing variable amounts of clinopyroxene and sporadically minor quartz. The proportion of primary pyroxenes decreases with increasing amphibole, whereas plagioclase modal amounts increase with decreasing abundance of ferromagnesian phases (in Table 1 compare samples: LHBL20, LHBL22, VFO3, VFO7, VFO8 and VFO9). Gabbronorites are often characterized by the development of planar high-temperature ductile foliation, sporadically preserve igneous layering, and are sometimes intruded by a suite of massive fine-grained mafic sills and dikes. Gabbronorites are hypidiomorphic, coarse-grained, and have variable modal proportions of plagioclase, which is commonly the most abundant phase (Table 1). Sometimes, plagioclase concentrated in monomineralic domains shows triple junction among crystals. Some gabbros contain cumulus crystals of orthopyroxene and/or clinopyroxene that appear as patchy clusters with interstitial subhedral plagioclase. In contrast, most gabbros show that pyroxenes grew late in the inter-cumulus in plagioclase-dominated layers. Within the gabbroic rocks, crystal-settling has locally generated mm-thick layering. The presence of lens-shaped bodies dominated by either plagioclase or a combination of amphibole and orthopyroxene is taken to indicate that gravity-driven mineral separation led to differentiate igneous rocks at meter scale. At the thin section scale, much of the original igneous relationships were modified by amphibole overgrowing at a late-magmatic stage and/or under subsolidus conditions (Fig. 2B and C). Most typical gabbronorite shows pseudo-polygonal to lobate textures associated to post-magmatic overprinting. Amphibole appears as large crystals with irregular shapes (sometimes skeletal or poikilitic) that formed surrounding orthopyroxene and clinopyroxene. These textures indicate that pyroxenes were in reaction with melt to produce amphibole (Fig. 2B and C). Apatite occurs as euhedral grains or tiny needles and appears enclosed by, or interstitial among, early-crystallizing rock-forming minerals. Oxides are chiefly separate crystal with subhedral or anhedral habits.

Diorites bearing orthopyroxene and having variable amounts of quartz (samples LHLB1, VFO1A, VFO6), occur as lens-shaped bodies among the gabbronoritic rocks. In the Sierra La Huerta, a diorite-dominated body is so large that it has been mapped at a regional scale (e.g. Vujovich et al., 1996, Fig. 1). Less-evolved chilled inclusions (enclaves) in diorites (LHBL6; VFO1B) are amphibole gabbros that petrographically resemble the rocks of the fine-grained mafic dikes. Typical diorites are medium- to coarse-grained and present subhedral to anhedral inequigranular texture. They are dominated by plagioclase and amphibole, but always contain variable proportions of orthopyroxene, biotite, and quartz, and minor oxides, apatite, zircon, and sporadic clinopyroxene. The diorites typically show evidence for having experienced solid-state deformation, which becomes more marked with increasing quartz abundance. Large grains of quartz have undulose extinction, internal subgrains, and irregular-shaped cuspate habits. Aggregates of quartz form bands that wrap around plagioclase and amphibole. Igneous plagioclase is bent and variably re-crystallized. Highly-strained diorites have plagioclase-rich pseudo-polygonal textural domains implying that dynamic reworking was not complete or mineral recovery partly healed the microstructures.

Layered ultramafic/mafic cumulate rocks form hundred-m-thick lens-shaped bodies that are enclosed within gabbronorites were reported by Mirré (1976) in the Jaboncillo valley (VFJA7). Several bodies of cumulate rocks have been found within the mafic unit and near the transition between mafic and supracrustal metamorphic units. Most of the layered mafic/ultramafic rocks are amphibole-bearing olivine-plagioclase cumulate rocks (Fig. 3A).

Please cite this article in press as: Otamendi, J.E. et al., Geology and petrology of a deep crustal zone from the Famatinian paleo-arc, Sierras ..., J. S. Am. Earth Sci. (2009), doi:10.1016/j.jsames.2008.11.007

Table 1B
Whole-rock trace element analyses of rock from Sierras La Huerta-Valle Fértil.

Sample	Mafic unit											
	LHBL1	LHBL5	LHBL6	LHBL20	LHBL22	LHBL23	LHBL25	VFJA7	VFCA1A	VFCA1B	VFCA4A	VFCA4B
XRF (ppm)												
V	306	131	316	148	324	89	120	79	264	355	298	132
Cr	42	31	99	225	54	77	72	1355	35	55	54	29
Co	63	67	46	76	60	38	89	96	51	51	51	90
Ni	16	15	38	429	95	73	29	407	18	35	38	9
Cu	111	37	124	9	184	63	121	76	58	249	55	17
Zn	83	82	139	60	87	66	78	59	123	118	124	70
Ba	151	286	85	271	113	466	609	52	120	78	106	192
Nb	10	9	10	3	4	8	7	3	8	5	4	7
Rb	41	28	4	22	5	29	37	4	10	5	2	11
Sr	192	214	198	137	123	238	187	163	234	164	238	201
Y	27	20	65	12	24	39	7	4	18	25	18	8
Zr	45	196	51	47	46	626	398	27	50	50	48	230
ICP-MS (ppm)												
Sc	33.5	19.0	49.1	22.9	46.7	20.4	15.4	67.1	29.9	56.6	50.7	22.0
Nb	8.6	8.7	8.5	1.5	2.3	6.2	5.2	0.6	9.5	3.3	2.9	7.0
Cs	1.6	0.4	0.3	0.2	0.1	0.01	0.3	0.2	0.8	0.2	0.2	0.3
La	11.1	17.5	13.9	1.9	3.2	32.1	24.2	2.0	19.2	9.0	11.7	15.7
Ce	24.6	37.5	40.6	4.9	8.6	66.5	41.0	4.3	39.7	24.0	27.2	29.1
Pr	3.3	5.1	7.0	0.6	1.2	9.9	4.5	0.5	5.3	3.7	3.8	3.3
Nd	14.7	21.8	34.5	3.4	6.4	43.6	16.2	2.0	21.8	16.2	16.2	12.1
Sm	3.7	4.7	9.5	0.9	1.9	9.6	2.1	0.5	4.7	4.3	3.9	2.0
Eu	0.9	1.5	2.1	0.4	0.8	2.1	1.5	0.2	1.7	1.5	1.3	1.3
Gd	4.1	4.9	10.3	1.3	2.7	9.5	1.6	0.5	4.6	4.8	4.0	1.7
Tb	0.7	0.7	1.7	0.2	0.5	1.3	0.2	0.1	0.7	0.8	0.7	0.2
Dy	4.6	3.9	10.7	1.5	3.3	7.1	0.8	0.5	4.1	5.3	4.0	1.4
Ho	1.0	0.7	2.2	0.4	0.7	1.3	0.2	0.1	0.9	1.1	0.9	0.3
Er	2.7	1.8	6.0	0.9	2.0	3.2	0.4	0.3	2.4	3.1	2.4	0.8
Tm	0.4	0.2	0.9	0.1	0.3	0.4	0.1	0.1	0.3	0.4	0.3	0.1
Yb	2.6	1.3	5.6	0.9	1.9	2.1	0.4	0.3	2.1	2.8	2.2	0.8
Lu	0.4	0.2	0.8	0.2	0.3	0.3	0.1	0.1	0.3	0.4	0.3	0.1
U	0.4	0.3	0.1	0.05	0.1	bdl	bdl	0.1	0.2	0.2	0.2	0.2
Th	1.0	1.0	0.3	0.1	0.2	4.4	1.8	0.4	1.1	0.7	0.9	0.9
Pb	7.4	4.9	2.1	2.4	3.1	8.2	3.6	2.6	11.1	6.9	8.3	9.8

Sample	Mafic unit										
	VFO1A	VFO1B	VFO3	VFO4A	VFO4B	VFO6	VFO7	VFO8	VFO9	VFO10B	VFO12
XRF (ppm)											
V	214	273	163	376	265	228	440	306	376	103	116
Cr	55	316	342	71	53	45	52	121	93	19	18
Co	51	45	25	51	44	53	46	56	48	62	50
Ni	24	111	54	39	16	15	15	71	23	0.3	3
Cu	53	71	77	154	52	55	132	91	100	2	15
Zn	92	115	22	124	137	117	154	121	143	65	74
Ba	394	170	52	65	169	203	71	62	62	42	115
Nb	11	9	3	4	10	9	8	6	8	5	10
Rb	58	30	4	3	6	13	3	2	2	2	3
Sr	187	125	216	156	236	235	182	158	171	197	259
Y	43	40	15	19	33	28	34	27	38	15	31
Zr	156	54	47	40	203	180	72	57	73	426	213
ICP-MS (ppm)											
Sc	26.6	28.7	16.3	38.7	24.1	22.9	38.1	36.5	45.9	16.2	14.9
Nb	8.1	5.1	0.8	1.8	6.5	5.8	4.5	3.2	6.6	1.7	5.3
Cs	0.6	0.2	0.2	0.03	0.1	0.3	0.02	0.02	0.02	0.01	0.03
La	16.2	17.6	1.4	4.2	10.5	9.7	8.6	8.5	11.2	3.7	9.2
Ce	42.1	49.2	3.1	11.3	25.0	23.3	22.4	22.8	33.5	9.2	22.0
Pr	6.8	7.5	0.4	1.8	3.7	3.5	3.4	3.5	5.6	1.4	3.3
Nd	30.2	28.7	1.8	8.7	16.0	15.1	14.6	14.5	24.7	6.4	14.7
Sm	7.5	5.8	0.5	2.5	3.8	3.6	3.5	3.4	5.8	1.6	3.5
Eu	1.4	1.4	0.2	0.9	1.0	1.1	0.9	1.1	1.6	0.5	1.0
Gd	7.6	5.1	0.4	2.9	3.8	3.6	3.6	3.4	5.8	1.7	3.5
Tb	1.3	0.8	0.1	0.5	0.6	0.6	0.6	0.6	1.0	0.3	0.5
Dy	7.2	4.7	0.4	3.1	3.6	3.4	3.6	3.5	5.6	1.5	3.2
Ho	1.5	1.0	0.1	0.7	0.8	0.7	0.8	0.7	1.2	0.3	0.7
Er	3.9	2.8	0.3	1.9	2.1	1.9	2.0	2.0	3.3	0.8	1.8
Tm	0.6	0.4	0.04	0.2	0.3	0.3	0.3	0.3	0.5	0.1	0.2
Yb	3.2	2.8	0.3	1.7	1.8	1.7	1.8	1.9	3.1	0.7	1.5
Lu	0.5	0.4	0.03	0.2	0.3	0.3	0.3	0.3	0.5	0.1	0.2
U	0.2	0.4	0.1	0.1	0.2	0.2	0.1	0.1	0.02	0.1	0.1
Th	0.7	2.0	0.3	0.5	0.6	0.5	0.4	0.2	0.1	0.1	0.2
Pb	7.7	4.9	2.2	2.2	3.4	3.9	3.7	2.0	2.6	2.0	3.6

Please cite this article in press as: Otamendi, J.E. et al., Geology and petrology of a deep crustal zone from the Famatinian paleo-arc, Sierras ..., J. S. Am. Earth Sci. (2009), doi:10.1016/j.jsames.2008.11.007

Table 1B (*continued*)

Sample	Intermediate tonalitic unit				Silicic granodioritic unit				
	GVF14	GVF15	GVF16	GVF17	GVF10	GVF11	GVF12	GVF30	GVF31
XRF (ppm)									
V	92	212	115	90	109	135	73	107	168
Cr	16	19	19	16	14	14	13	10	17
Co	54	44	53	64	75	60	67	50	39
Ni	4	4	3	3	3	5	3	7	4
Cu	29	55	17	9	22	27	24	14	47
Zn	77	113	70	61	68	92	58	66	117
Ba	363	429	457	434	408	267	399	356	318
Nb	11	11	12	10	13	13	16	12	11
Rb	72	59	71	72	100	121	126	85	61
Sr	227	243	216	203	195	187	136	283	344
Y	30	36	23	17	35	38	35	28	33
Zr	191	173	180	172	192	245	168	176	167
ICP-MS (ppm)									
Sc	16.0	20.7	10.6	7.0	17.8	17.2	13.7	18.5	33.0
Nb	8.4	7.7	7.1	6.7	12.1	12.3	15.4	8.7	10.7
Cs	1.1	0.5	0.8	1.0	2.4	3.0	2.9	3.1	2.7
La	22.6	16.5	10.6	8.3	33.7	22.0	29.8	28.3	28.7
Ce	46.8	40.5	22.9	18.9	64.7	51.8	58.7	51.2	59.1
Pr	6.4	6.0	3.2	2.7	8.6	7.8	7.5	6.6	9.0
Nd	24.7	24.1	12.6	10.5	34.5	35.3	27.6	23.6	34.9
Sm	5.1	5.3	2.8	2.3	6.7	7.6	6.0	4.7	7.6
Eu	1.2	1.4	0.7	0.7	1.3	1.6	1.2	1.5	2.0
Gd	4.9	5.1	2.8	2.2	6.4	7.2	5.9	4.5	7.3
Tb	0.8	0.8	0.4	0.4	1.0	1.1	1.0	0.7	1.1
Dy	4.6	4.7	2.6	2.1	6.0	6.6	6.1	4.0	6.5
Ho	1.0	1.0	0.6	0.4	1.3	1.4	1.4	1.0	1.6
Er	2.7	2.7	1.6	1.3	3.5	3.9	3.8	2.5	4.0
Tm	0.4	0.4	0.2	0.2	0.5	0.6	0.6	0.4	0.6
Yb	2.4	2.4	1.4	1.3	3.4	3.7	3.7	2.1	3.5
Lu	0.4	0.4	0.2	0.2	0.5	0.5	0.6	0.3	0.5
U	0.4	0.5	0.3	0.5	1.3	0.8	1.8	0.6	0.9
Th	3.1	1.5	1.2	1.0	8.6	2.1	14.6	5.7	4.1
Pb	9.5	5.9	4.8	6.8	9.0	7.7	14.5	22.6	17.2

Sample	Supracrustal metasedimentary rocks and anatectic leucogranites							
	LHBL41	LHBL43	LHBL44	VFO2A	VFO11	VFO2C	LHBL26	LHLB46
XRF (ppm)								
V	105	160	111	170	121	9	24	14
Cr	76	122	86	129	107	7	18	8
Co	115	79	137	61	67	132	200	180
Ni	31	56	36	62	49	5	2	21
Cu	55	4	6	5	4	4	9	111
Zn	75	81	56	166	87	11	15	11
Ba	314	554	371	645	623	1874	2306	286
Nb	13	17	16	18	16	2	4	4
Rb	55	76	51	145	55	71	76	28
Sr	119	88	83	145	177	263	255	168
Y	22	35	41	27	33	7	8	4
Zr	265	315	582	217	336	108	105	142
ICP-MS (ppm)								
Sc	12.2	12.9	10.6	11.6	8.2	1.2	1.7	0.8
Nb	12.1	16.5	14.3	12.2	8.6	1.3	1.7	1.4
Cs	2.5	4.4	1.9	1.7	0.3	0.6	1.2	0.2
La	34.0	47.4	46.8	35.8	32.5	21.4	20.6	34.5
Ce	66.5	90.2	90.0	72.3	64.5	37.2	35.6	62.1
Pr	9	13.0	12.8	9.4	8.5	4.4	4.0	7.7
Nd	35.8	51.8	51.4	33.8	30.6	14.8	14.7	29.0
Sm	6.8	10.1	9.9	6.2	5.6	2.5	2.8	3.3
Eu	1.3	1.9	1.8	1.3	1.1	2.1	2.4	1.5
Gd	5.9	8.7	8.7	5.0	4.5	2.1	1.8	1.4
Tb	0.8	1.2	1.2	0.7	0.6	0.3	0.3	0.1
Dy	4.2	6.6	6.9	3.2	2.8	1.2	1.4	0.3
Ho	0.7	1.3	1.3	0.6	0.4	0.2	0.3	0.1
Er	1.7	3.3	3.6	1.3	0.9	0.4	0.6	0.1
Tm	0.2	0.5	0.5	0.2	0.1	0.04	0.1	0.02
Yb	1.2	2.5	3.0	0.9	0.5	0.2	0.5	0.05
Lu	0.2	0.4	0.4	0.1	0.1	0.03	0.1	0.02
U	0.4	0.3	0.5	1.4	0.8	bdl	bdl	bdl
Th	13.5	18.2	3.7	14.2	12.9	9.1	2.5	8.6
Pb	6.8	8.0	7.2	23.9	10.2	7.4	17.0	4.8

bdl, below detection limit.

Please cite this article in press as: Otamendi, J.E. et al., Geology and petrology of a deep crustal zone from the Famatinian paleo-arc, Sierras ..., J. S. Am. Earth Sci. (2009), doi:10.1016/j.jsames.2008.11.007

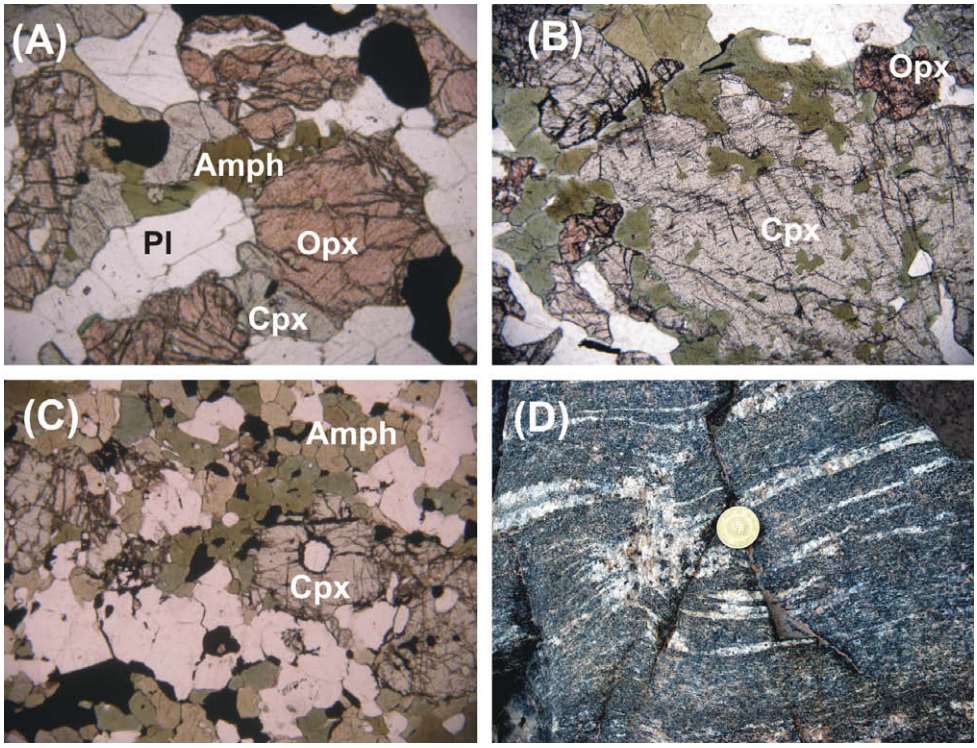

Fig. 2. (A) Photomicrograph of a two pyroxene gabbro showing the typical igneous texture in which pyroxene, plagioclase and oxide occur as subhedral crystals and amphibole overgrows pyroxene rims. (B) Photomicrograph illustrating the replacement of clinopyroxene and orthopyroxene by green amphibole. (C) Photomicrograph of an amphibole gabbro showing that pyroxenes have been extensively replaced by small amphibole crystals. Pseudo-polygonal domains and amphibole triple-grain junctions suggest textural reworking at sub-solidus conditions. All photomicrographs (A, B and C) were obtained under plane-polarized light and their long dimension is 0.25 cm. (D) Mafic stromatic migmatite with tonalitic leucosomes located in boudin necks and in layers parallel to the foliation defined by mineral preferred orientation of amphibole.

The cumulate rocks are composed of variable proportions of olivine with interstitial plagioclase (Fig. 3B). Cumulate usually contains large amounts of pyroxenes and amphibole, and always bears variable and subordinate amounts of oxide and spinel. Plagioclase appears concentrated in clusters evenly distributed within the olivine cumulate. The presence of coronitic reaction texture in these rocks has drawn attention from several authors (e.g. Baldo et al., 1999; and references therein). The most common coronas display the sequence olivine/orthopyroxene rim/orthopyroxene + spinel symplectite/amphibole/amphibole + spinel symplectite/plagioclase (Fig. 3C). In these cumulate rocks, olivine, plagioclase and chromian magnetite are the dominant igneous minerals. Other minerals that could have crystallized from the magma are: (1) inter-cumulus grains of orthopyroxene and clinopyroxene in olivine cumulates, and (2) dark-brown chromian spinel (picotite) enclosed in olivine and as euhedral separate grains (Fig. 3A).

Sill or dike bodies that intruded into the mafic unit are typically composed of massive and fine-grained amphibole gabbros (Fig. 3D; samples VFO4A, VFCA1B; VFCA4B). These gabbros have equigranular, hypidiomorphic textures with parallel alignment of amphibole and tabular plagioclase. However, the isotropic aspect of rocks and the strong mineral orientation aligned parallel to the sills' margins suggest that the fabric is due to magmatic flow (Nicolas, 1992). Sills and dikes are sharp-walled tabular-shaped bodies that turn and coalesce forming at m-scale either a net or a swarm within the gabbronoritic to dioritic rocks. Furthermore, some of these sill/dike bodies pass into swarms of chilled mafic inclusions in diorites, implying a genetic connection between sills and mafic inclusions (see Wiebe et al., 2002). In chilled mafic rocks, the dominant euhedral to subhedral texture and the modal proportions suggest that amphibole, plagioclase and magnetite crystallized almost without competing phases. Biotite often overgrows amphibole borders, and quartz is interstitial and spatially related to plagioclase. Apatite, either free or included in early crystallized phases, occurs as accessory mineral.

4.2. Intermediate igneous rock unit

This unit consists of heterogeneous associations of intermediate rocks containing multiple chilled mafic intrusions, including dikes and inclusions (microgranular enclaves). At regional-scale, the intermediate unit occurs as elongate belts of intrusions, spreading all over the length of the Sierras Valle Fértil-La Huerta (Fig. 1; and Mirré (1976)). Such elongate plutonic bodies do not form a typical batholith; rather, the plutonic tonalites that dominate and characterize the unit are a complexly interlayered sequence of igneous mafic rocks and metasedimentary migmatites. It should be noted that within the intermediate unit, the abundance of migmatitic layers and/or septa progressively decreases towards the transitional boundary with the granodiorite-dominated silicic unit. Observed at outcrop scale, the tonalites show a well-developed foliation. Foliation is marked by parallel alignment of tabular plagioclase associated with prismatic amphibole and micas. The strong alignment of these igneous crystals indicates that the foliation is primarily magmatic. The primary foliation is parallel to both the mafic sills and the alignment of enclaves occurring as either individual or swarm. In general, the magmatic foliation in the tonalites is partly reworked by subsolidus deformation. Irrespective of the nature, foliation is NNW-SSE-trending steeply-dipping and broadly parallel to the internal foliation in the interlayered metasedimentary and mafic belts (e.g. Mirré, 1976). However, the primary foliation together with the mafic inclusions appears locally bent, lying at a high angle with the regional scale foliation. While tonalites were intruded by mafic dikes, they behaved as an elastico-vis-

Please cite this article in press as: Otamendi, J.E. et al., Geology and petrology of a deep crustal zone from the Famatinian paleo-arc, Sierras ..., J. S. Am. Earth Sci. (2009), doi:10.1016/j.jsames.2008.11.007

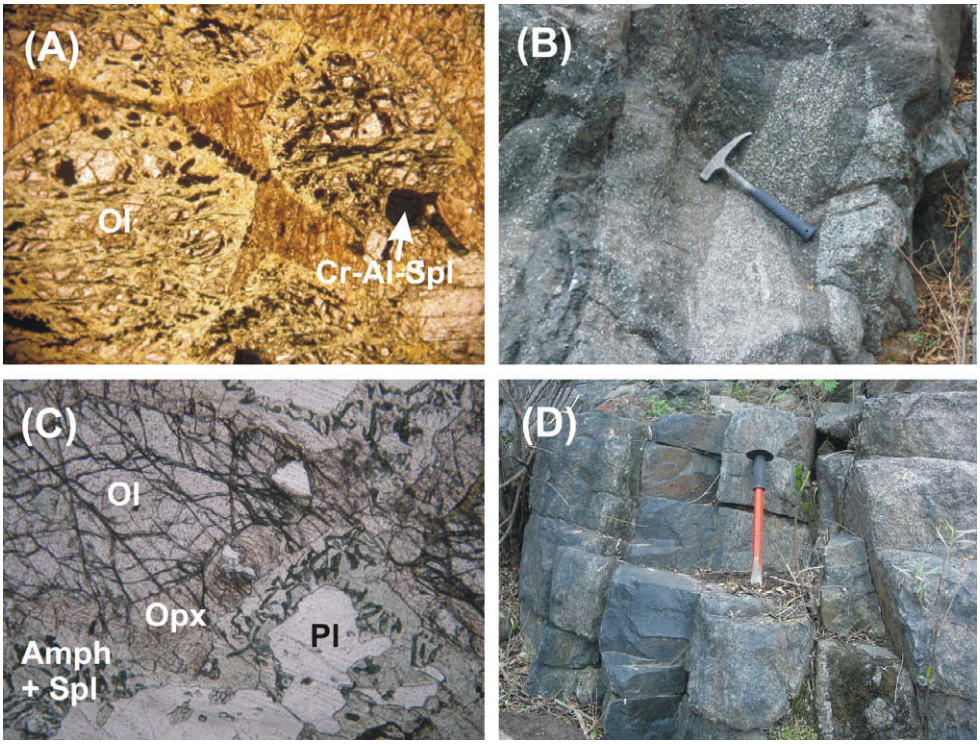

Fig. 3. (A) Photomicrograph of orthocumulate texture defined by euhedral olivine crystals with interstitial pyroxenes and amphiboles. Olivine is largely altered to serpentine and includes early picotite crystals. Plane-polarized light (long dimension is 0.25 cm). (B) Field photograph showing a section of the gabbroic cumulate. Igneous layers are distinguished by the concentration of plagioclase relative to mafic phases. The limits of layers are both sharp and gradation, and each layer exhibits grading from olivine-rich base to a plagioclase-rich top. (C) Photomicrograph of the olivine-plagioclase corona showing an inner rim of orthopyroxene and an outer rim of amphibole + spinel symplectite. Plane-polarized light (long dimension is 0.25 cm). (D) Tabular-shaped sill of fine-grained amphibole gabbro intruded into Pl-rich norite.

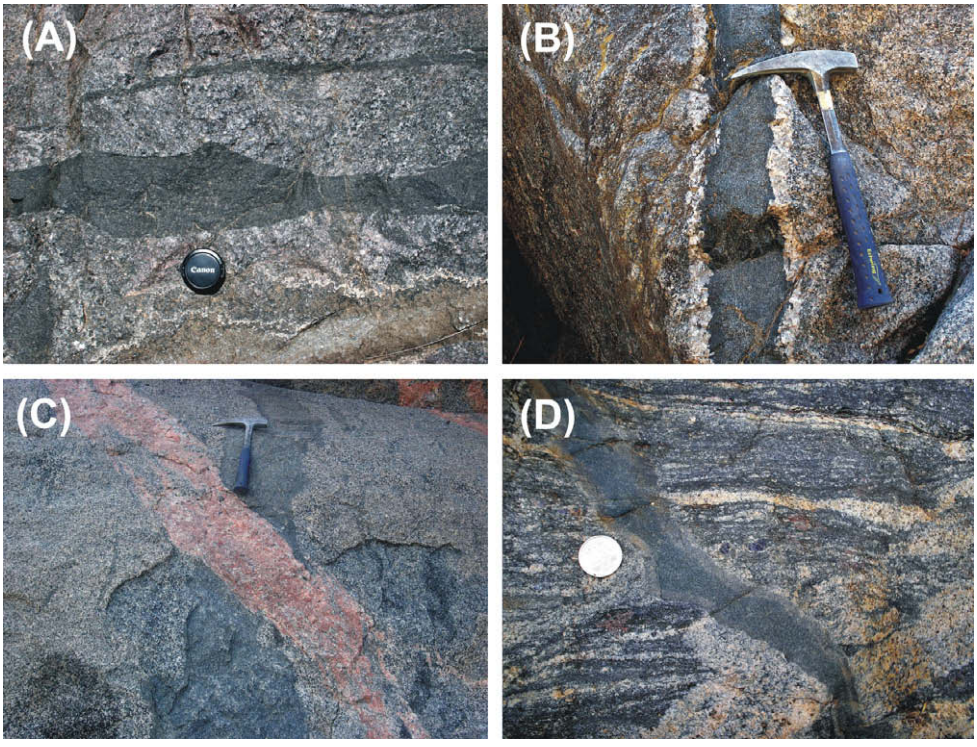

Fig. 4. Photographs showing the field relationships among mafic sill/dike and mafic inclusion within rocks from the intermediate (A) and (B), silicic (C), and supracrustal (D) units. (A) Mafic sill intruded into a tonalite from the intermediate unit, note that the pinch-and-swell geometry of the sill implies that the host rock behaved as an elastico-viscous material. (B) Mafic dike intruded into a tonalite from the intermediate unit. The presence of a coarse-grained Pl-rich band along the contact of the dike implies that heat and fluid released from the dike re-melted the tonalite. (C) Syn-magmatic swarm of microdioritic strips being partly assimilated by a tonalitic magma, whereas mingling between tonalite and late-magmatitic leucogranitic dikes locally produce granodioritic lenses. (D) Mafic dike intruded into a metapelitic migmatite from the supracrustal unit. The margins of the dike are chilled and chemically modified by interaction with the migmatite host. The timing of the mafic intrusion is also shown by the observation that the dike cuts across the foliation-parallel leucosomes already segregated in the migmatite.

Please cite this article in press as: Otamendi, J.E. et al., Geology and petrology of a deep crustal zone from the Famatinian paleo-arc, Sierras ..., J. S. Am. Earth Sci. (2009), doi:10.1016/j.jsames.2008.11.007

cous material (Fig. 4A). Moreover, tonalite appears re-melted along the contact with the chilled mafic intrusive (Fig. 4B) suggesting that the tonalites were still experiencing temperatures close to their solidus when they were repeatedly intruded by mafic dike/sill bodies. Weak to moderate solid-state high-temperature overprint is recorded by large irregular grains and sutured aggregates of quartz that are elongated parallel to the magmatic foliation. Up to two generations of igneous plagioclases occasionally show deformation twins and are variably re-crystallized to small-sized grains. Typical tonalites are medium- to coarse-grained, equigranular, and hypidiomorphic, with plagioclase and quartz as dominant phases but always bearing amphibole and biotite (see Table 1). Plagioclase usually forms subhedral grains with tabular habits that define the magmatic foliation, and sporadically includes euhedral amphibole crystals. Accessory minerals include opaque oxides, zircon, apatite, epidote, allanite, and sphene. Epidote is euhedral, sometimes allanite-cored, and remarkably widespread. Sphene is normally euhedral but corroded, and less abundant than epidote.

4.3. Silicic igneous rock unit

In the inferred root zones of the silicic unit, the tonalite-dominated unit passes to a granodiorite batholith through a transitional zone, which is up to 2-km wide. This boundary zone separating tonalite-dominated and granodiorite-dominated units is characterized by mingling of tonalitic and leucogranitic magmas, which together appear multiply-intruded by pod- and dike-like bodies of amphibole gabbros. At hand specimen scale, the typical granodiorite dominating this unit is a medium-grained rock with either an inequigranular texture or a porphyritic K-feldspar texture. The granodiorite commonly has a roughly NNW-SSE striking steeply dipping igneous foliation. The granodiorite contains elongate microdioritic enclaves, which occur as either individual inclusions (GVF11 is a representative sample) or tabular-shaped swarms of multiple inclusions (Fig. 4C). Microdioritic enclaves are widespread and they represent a distinctive feature of these granodiorites. They are elongate and lenticular, often with sharp lobate or crenulate contacts. Some inclusions exhibit a very elongate shape passing into a schlieren-like trail of fine-grained microdioritic material, which is also extended parallel to the foliation in granodiorite (e.g. Castro et al., 2008). Microdioritic inclusions are widely spaced in some zones within the granodiorites. These inclusions are identical to those forming swarms but tend to be smaller. Latter features provide evidence for the idea that a significant amount of microdioritic inclusions were digested and incorporated into the evolving granodioritic magmas (e.g. García-Moreno et al., 2006). Within the granodiorite-dominated unit, there are large amphibole gabbroic bodies. The granodiorites also include meter-scale blocks of stromatic metasedimentary migmatites, and are widely intruded by leucogranitic veins. Weakly zoned plagioclase crystals tend to be subhedral. K-feldspar occurs as irregular lath-shaped grains with inequigranular texture or as subhedral tabular megacrystals in porphyritic granodiorite. Granodiorites always have pale reddish–brown biotite coexisting with green prismatic amphibole; they commonly contain epidote, apatite, sphene, oxide, allanite and zircon as accessory phases.

4.4. Supracrustal sedimentary-derived metamorphic rock unit

This unit is dominated by migmatites derived from siliciclastic protoliths and formed during granulite-facies metamorphism. Marble/calcsilicate/amphibolite rocks locally occur as lens-shaped belts and are interpreted to have been part of a sedimentary sequence (Otamendi et al., 2008). Metatexite, which is the most abundant morphology among the migmatites, commonly has a well-developed layering that results from *in situ* segregation of leucosomes parallel to the foliation preserved in the mesosomes. The timing of leucosome generation in migmatites is clearly deduced from field relations. Discordant anatectic leucogranites, which are drained after coalescence of leucosomes in migmatites, cross cut layered gabbronoritic bodies. In contrast, some chilled mafic dikes cut across the migmatites after extensive melting has occurred (Fig. 3D). Field relationships thereby indicate that the paragneissic migmatites were partially melted broadly coeval with the progressive intrusion of mafic magmas.

At a regional scale, the migmatites show compositional signature inherited from their sedimentary precursor. The migmatites display a wide variety of mineral proportions and assemblages among which garnet-cordierite-sillimanite-rich metapelite and garnet-poor to garnet-absent quartzo-feldspathic metagreywacke are the end-members (Otamendi et al., 2008). Hence, the mesosomes consist of quartz + plagioclase + biotite with a variable combination of garnet ± cordierite ± sillimanite ± K-feldspar ± Al-rich spinel. Irrespective of the mineral assemblage in the mesosome, the leucosomes are largely leucogranitic and essentially made up of quartz and K-feldspar, with lesser amounts of plagioclase ± garnet ± cordierite. Felsic K-feldspar-rich granites are interpreted to have crystallized from magmas generated after partial melting and melt segregation from metasedimentary migmatites. Some anatectic leucogranitic magmas feed sharp-walled lens-shaped bodies without interacting with other lithologies. Many K-feldspar-rich anatectic granites appear also mixed with amphibole gabbros, tonalites and granodiorites.

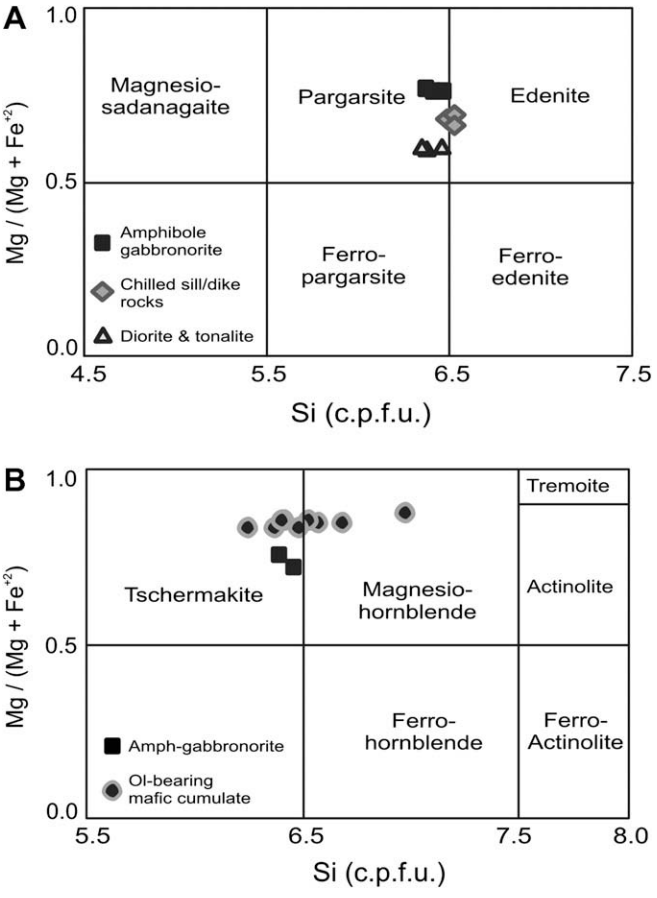

Fig. 5. Nomenclature of amphibole after Leake et al. (1997). (A) Classification of the calcic amphiboles with $Ca_B > 1.5$ and $(Na + K)_A \geqslant 0.5$. (B) Classification of the calcic amphiboles with $Ca_B > 1.5$ and $(Na + K)_A < 0.5$.

Please cite this article in press as: Otamendi, J.E. et al., Geology and petrology of a deep crustal zone from the Famatinian paleo-arc, Sierras ..., J. S. Am. Earth Sci. (2009), doi:10.1016/j.jsames.2008.11.007

5. Mineral chemistry

5.1. Analytical procedures

Electron microprobe analyses were conducted at the University of Huelva Spain using a JEOL JXA-8200 Superprobe equipped with four wavelength dispersive X-ray spectrometers. Two spectrometers are equipped with LIFH and PETH crystals, and the two others combined a distinct set of LIF, PETJ, TAP, LDE1, LDE2 and LDEB crystals. Counting times for each element were between 10 and 30 s at an accelerating potential of 15 kV. A beam current of 20 nA and width of around 5 μm. Mineral compositions were tested using stoichiometric constraints. Both natural and synthesized materials were used as standards. Mineral compositions are available as Supplementary material files.

5.2. Plagioclase

In the olivine-bearing gabbroic cumulate (VFJA7) plagioclase is highly calcic and fairly homogeneous; in the compositional range An >95% (symbols for minerals are after Kretz, 1983). Plagioclase in amphibole gabbronorites (VFO9) is less calcic and also compositionally homogenous, ranging from An_{91} to An_{87}. Plagioclase in a chilled mafic dike (VFCA1B) is slightly less calcic (An_{84}) than in the amphibole grabbronorite. High magmatic water content and low crystallization pressure are thought to be responsible for crystallization of such calcic plagioclase in mafic igneous rocks (Arculus and Wills, 1980). The anorthite mole fraction of plagioclase decreases nearly continuously from diorites (An_{66} to An_{48}) to granodiorites. Furthermore, in the granodiorites plagioclase is zoned from An_{46} in the core to An_{22} in some rims (as measured in the specimen GVF30).

5.3. Amphibole

Calcic clinoamphibole is together with plagioclase the most abundant phase in the studied igneous rocks (Fig. 5A). Amphiboles in the olivine-bearing cumulate rocks are mainly magnesio-hornblende with some tschermakite component (Fig. 5B). These amphiboles have high Mg-numbers (=100 Mg/Mg + Fe^{+2}) from 82 to 87,

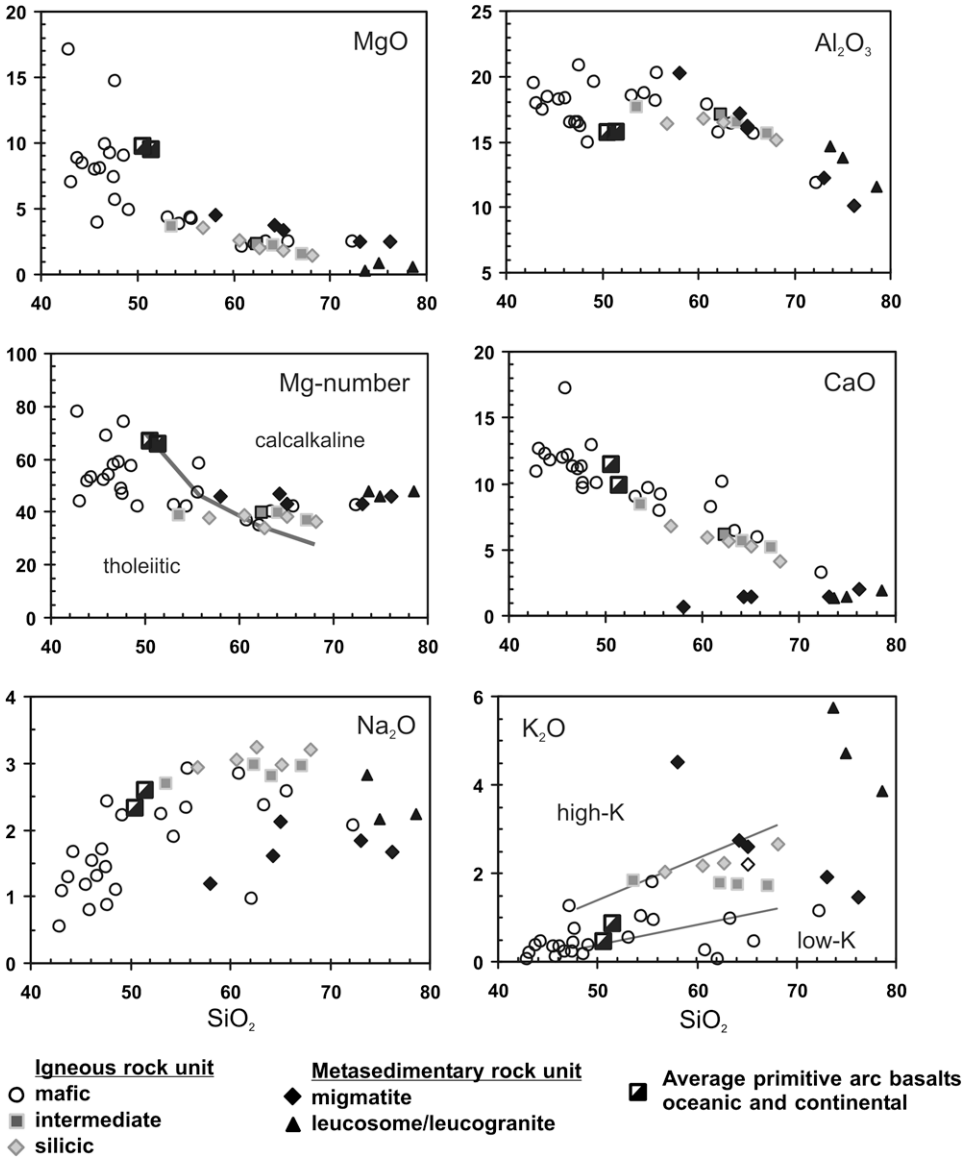

Fig. 6. Major element composition of each lithologic unit projected versus SiO_2 content. In the Mg versus SiO_2 diagram, the line dividing tholeiitic and calc-alkaline fields is from Miyashiro (1974) but after converting FeO^*/MgO ratio to Mg-number. The K_2O diagram shows the boundaries among low-K, medium-K and high-K after Le Maitre (1989). Composition of average primitive continental and oceanic arc basalts are taken after Kelemen et al. (2003).

Please cite this article in press as: Otamendi, J.E. et al., Geology and petrology of a deep crustal zone from the Famatinian paleo-arc, Sierras ..., J. S. Am. Earth Sci. (2009), doi:10.1016/j.jsames.2008.11.007

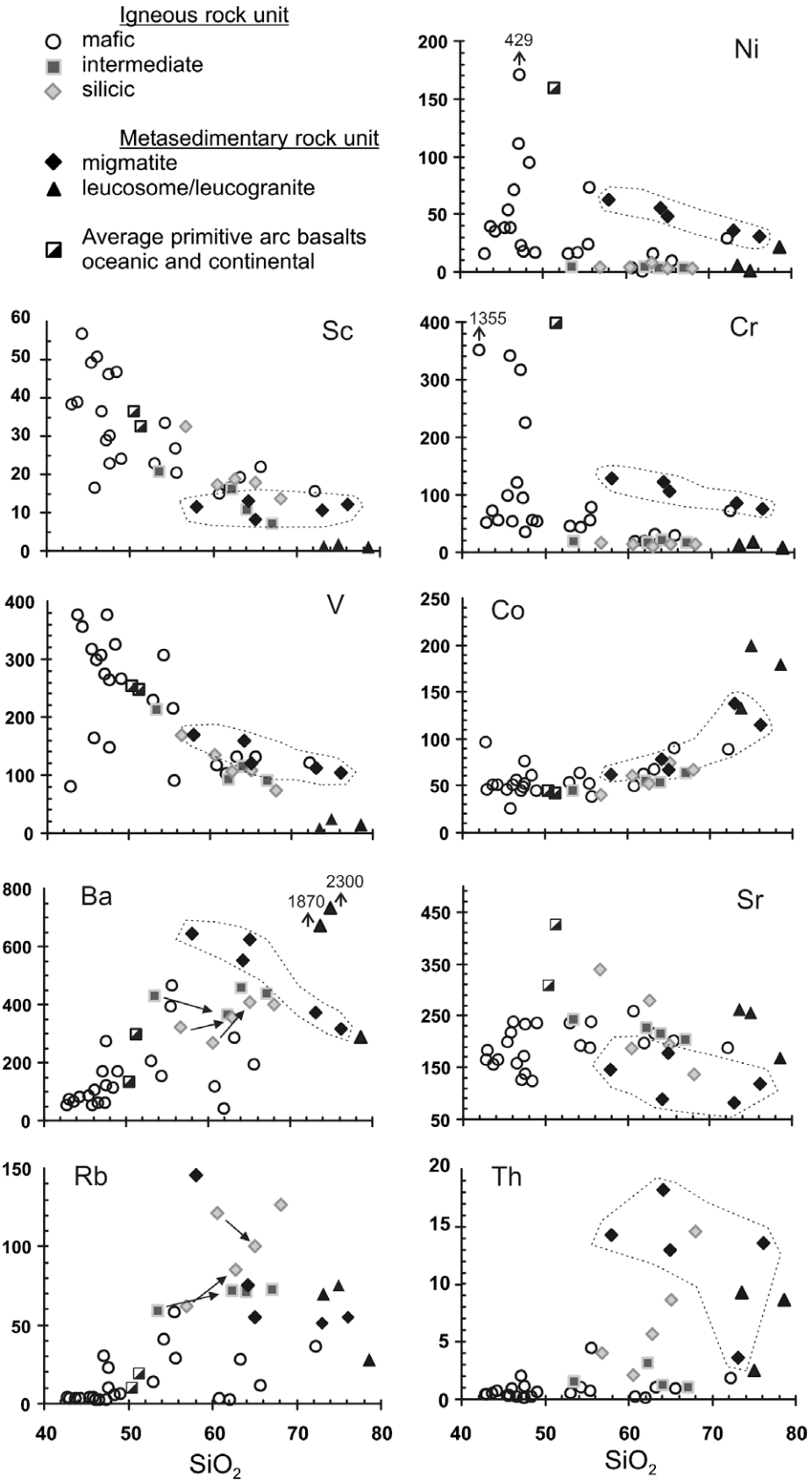

Fig. 7. Selected trace element contents plotted against SiO_2. The compositional field of supracrustal migmatites is outlined with a dashed line. In Rb and Ba diagrams arrows show the compositional relationships between microgranular inclusions and their host igneous rocks.

and a variable SiO_2 range (6.25–6.97 c.p.f.u., cations per formula unit). Cumulate-forming amphiboles also have significant Al_2O_3 contents (2.06–2.61 c.p.f.u.). In contrast, amphiboles from amphibole gabbronorite (specimen VFO9) have Mg-numbers of around

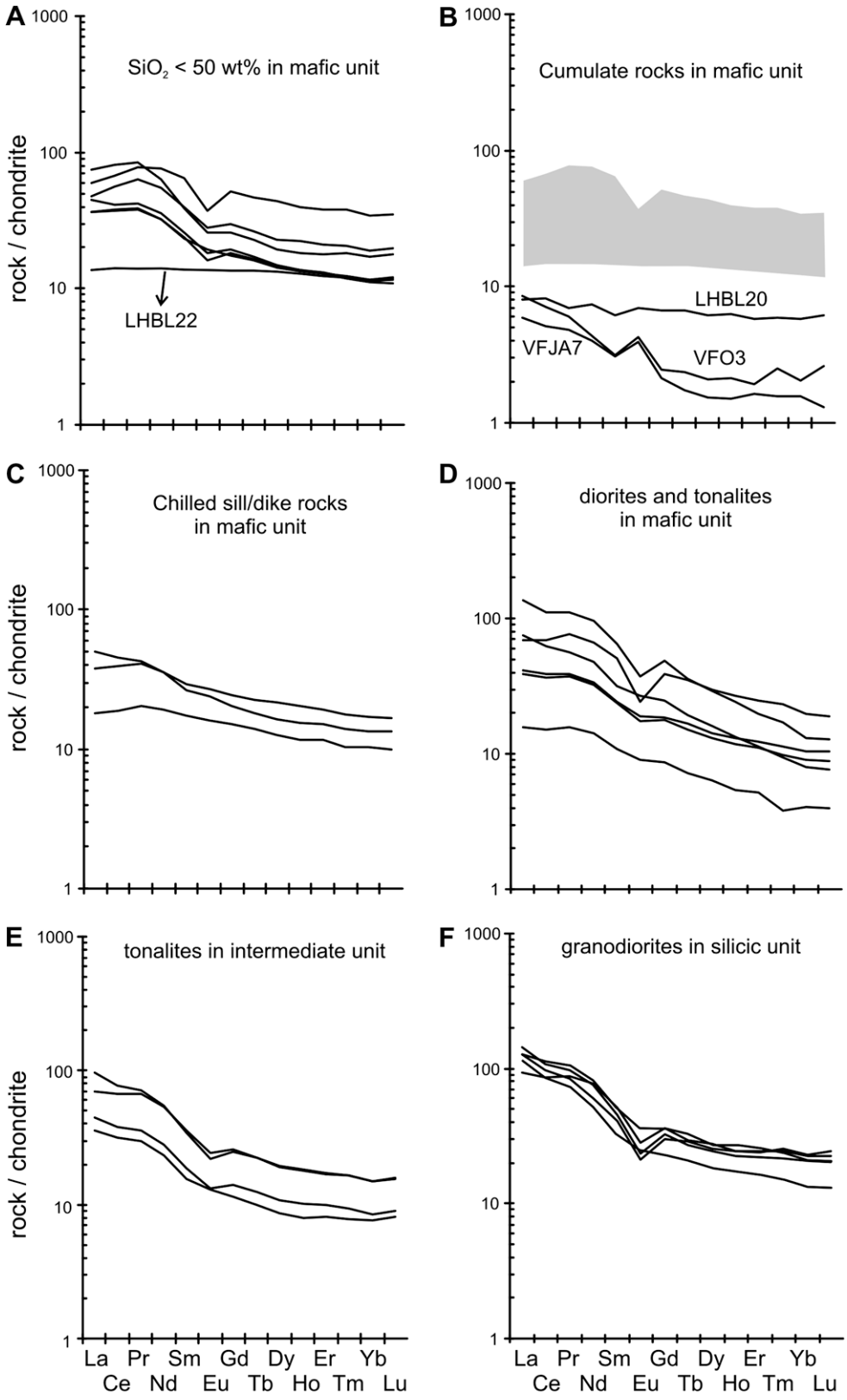

Fig. 8. Rare earth element abundances of igneous rocks from the Sierras de Valle Fértil-La Huerta, normalized to C1 chondrite Anders and Grevesse (1989). (A) Gabbronorites from mafic unit. (B) Pl- and olivine-bearing cumulate rocks from the mafic unit. The field for gabbronorites is shown in grey. (C) Chilled sill/dikes amphibole-rich gabbros from the mafic unit. (D) Diorites and tonalites from the mafic unit. (E) Granodiorites from the silicic unit. (F) Typical tonalites from the intermediate unit.

72, show a restricted SiO_2 range (6.35–6.53 c.p.f.u.) and are poorer in Al_2O_3 abundance (1.93–2.16 c.p.f.u.). Amphiboles from fine-grained mafic dike are similar to those in gabbronorites (Fig. 5A). A common characteristic of amphibole in gabbronoritic as well as dioritic rocks is that Na and K concentrations allocated in A sites are higher than 0.5 (c.p.f.u.). This feature determined that amphi-

Please cite this article in press as: Otamendi, J.E. et al., Geology and petrology of a deep crustal zone from the Famatinian paleo-arc, Sierras ..., J. S. Am. Earth Sci. (2009), doi:10.1016/j.jsames.2008.11.007

boles from amphibole gabbronorite, chilled mafic dike and diorite are pargarsitic. Some amphiboles in the chilled dikes show a weak edenitic component (Fig. 5A).

5.4. Orthopyroxene, olivine, biotite and Fe-Ti oxides

Orthopyroxene appears in olivine-bearing gabbroic cumulate, gabbronorites and less evolved diorites. In the gabbroic cumulates (specimen VFJA7), the orthopyroxene occurs rimming olivine (Fig. 3C). This is likely the reason that orthopyroxene has the same Mg-numbers (80–82) as olivine. In the amphibole gabbronorite, orthopyroxene Mg-numbers (70–72) are nearly identical to those of amphibole. Orthopyroxenes from cumulate rocks usually contain Al_2O_3 between 3 and 4 wt.%, whereas orthopyroxenes from amphibole gabbronorite (as measured in specimen VFO9) have Al_2O_3 contents lower than 2.5 wt.%.

Olivine occurs only in cumulate rocks (Fig. 3A and C), is partly resorbed and rimmed by orthopyroxene. Olivine Mg-number varies little at around 80.5 ± 0.5. This olivine composition (Fo *ca.* 80%) coexisting with highly calcic plagioclase (An >95%) has been shown to indicate that gabbroic cumulate formed in magmatic arc settings (Arculus and Wills, 1980; Beard, 1986).

Micas analyzed in a granodiorite (GVF30) consist of biotites that have Mg-numbers varying from 0.58 to 0.55, and total aluminum contents ranging between 1.50 and 1.56 c.p.f.u. TiO_2 content in these biotites is rather uniform 2.3–3.0 wt.%.

The maximum magnetite mode is found in the fine-grained mafic dikes (Table 1A). Chromian magnetite is present in olivine-bearing cumulate rocks; these magnetites contain around 4.7 wt.% of Cr_2O_3. Magnetite and ilmenite coexist in few amphibole gabbronorites. Ilmenite contains significant amounts of Fe (hematite fraction *ca.* 0.1) but magnetite have little ulvospinel mole fraction <0.01.

6. Whole-rock chemistry

6.1. Sampling approach and method

Forty samples from the four studied localities and covering all major lithologic units were analyzed for major and trace element concentrations (Table 1). Whole-rock chemical analyses were carried out on representative rocks of every lithologic unit. Each sample consists of 3–5 Kg of fresh material. After crushing the whole sample, approximately 500 g of homogenous pebble-sized material was pulverized within a tungsten-carbide grinding bowl. Major elements and selected trace elements (V, Cr, Co, Ni, Cu, Zn, Ba, Nb, Rb, Sr, Y, Zr, and Pb) were determined by X-ray fluorescence (XRF) at the Universidad de Oviedo, Spain, using glass beads and pressed powder pellets, respectively. Typical precision of the XRF technique is better than ±1.5% (relative). Trace elements, including some of those analyzed by XRF, were determined by inductively coupled plasma mass spectrometry (ICP-MS) at Universidad de

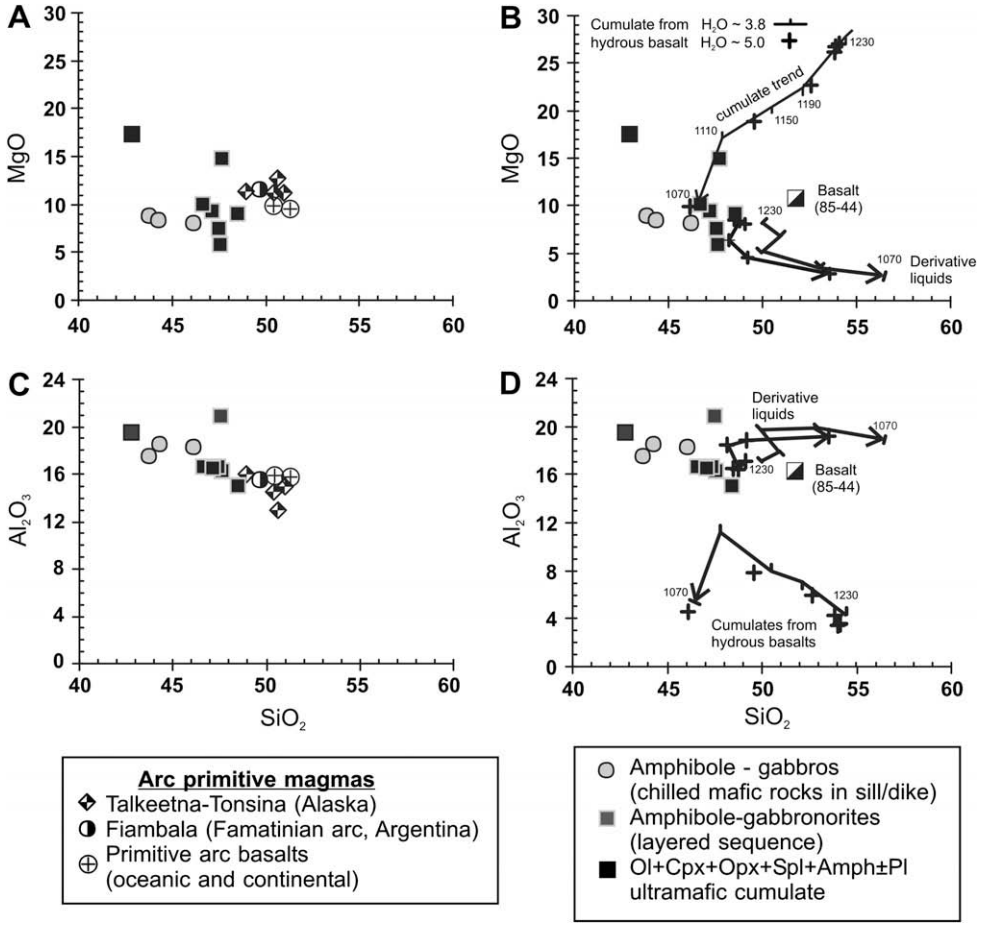

Fig. 9. (A and B) Major element composition as represented by $MgO–SiO_2$ (A) and $Al_2O_3–SiO_2$ (B) of igneous rocks from the mafic unit compared to primary basaltic arc magmas, including the worldwide estimates of continental and oceanic arcs Kelemen et al. (2003), and parental magmas from paleo-arc lower crustal sections exposed in southern Alaska DeBari and Sleep (1991) and northwestern Argentina DeBari (1994). Gabbronorite from Fiambalá (e.g. DeBari (1994)) represents another example of the lower crust of the Famatinian arc (see Fig. 1A). (C and D) The same major element variations as in diagrams A and B, is also projecting the glass compositions from crystallization experiments of hydrous basalt (e.g. Müntener et al. (2001)). Each corresponding solid assemblage bulk composition was estimated combining volume proportions and mineral compositions reported by Müntener et al. (2001). Numbers next to tick marks are temperatures reported for each experimental run.

Please cite this article in press as: Otamendi, J.E. et al., Geology and petrology of a deep crustal zone from the Famatinian paleo-arc, Sierras ..., J. S. Am. Earth Sci. (2009), doi:10.1016/j.jsames.2008.11.007

Huelva, Spain. The average precision and accuracy for most of these elements fall in the range of 5–10%, and they were controlled by repeated analysis of SARM-1 (granite) and SARM-4 (norite) international standard rocks of the South African Bureau of Standards (further details about ICP-MS determinations were presented by de la Rosa et al., 2001). Major elements are plotted onto diagrams after recalculating to 100% the sum of oxides on an anhydrous basis, and total Fe reported as Fe_2O_3 was converted to FeO to estimate Mg-numbers.

6.2. Characterization of igneous rock through major elements

Overall, the igneous rock samples vary over a wide range of SiO_2, displaying an almost continuous trend from olivine-bearing cumulate with around 43 wt.% to leucotonalites with nearly 72 wt.%. Modal quartz appears in rocks having SiO_2 abundance as low as 48–49 wt.% and its proportion increases following a strong positive correlation with the whole-rock SiO_2 content (Table 1). Gabbronoritic rocks mostly have SiO_2 contents below 50 wt.%, whereas diorites contain 52–56 wt.% of SiO_2 and tonalitic lenses from the mafic unit have up to 64 wt.% of SiO_2. Within the mafic unit, there is a considerable overlap in Al_2O_3, TiO_2, and Mg-number [=MgO/(MgO + FeO) on a molar basis obtained from whole-rock composition] among gabbronorites, diorites and tonalites (Fig. 6). In contrast, the chemical variation from gabbronorite through diorite to tonalite shows a broad but well-defined trend of decreasing MgO and CaO with increasing SiO_2 (Fig. 6). Considering rocks from the three igneous units, the abundance of CaO is not a simple indication of plagioclase proportion. The trend of CaO against SiO_2 also reflects the varying anorthite content in plagioclase and the modal amount of amphibole (Table 1A), as all these features decrease with increasing SiO_2. The less differentiated samples from the intermediate unit have major element contents mostly similar to those of the diorites and tonalites from the mafic unit.

Typical rocks from the intermediate unit generally have SiO_2 abundances higher than 60 wt.%, and they include microdioritic enclaves with the same composition as those of the diorites in the mafic unit. The concentration of SiO_2 in granodiorites overlaps with that of the more evolved tonalites. At the same SiO_2 abundance, the granodiorites have higher K_2O than the typical tonalites, which in turn contain more K_2O than tonalites interlayered within the mafic unit (Fig. 6).

In the Mg-number *versus* SiO_2 diagram, plutonic rocks from the three igneous units show a scattered trend that crosses the limit between tholeiitic and calc-alkaline field at about 55 wt.% of SiO_2 (Fig. 6). Although the existence of igneous trends crossing the limit between tholeiitic to calc-alkaline fields has been reported in plutonic and volcanic suites (Grove and Kinzler, 1986; Sisson et al., 1996), this is still an important observation for an igneous sequence of rocks closely associated in space and time. Remarkably, the Mg-number shows an ill-defined variation within the mafic rocks (SiO_2 <52 wt.%) but remains almost constant at *ca.* 0.40–0.45 through the SiO_2 range of intermediate and silicic rocks. Collectively, the igneous rocks have alumina saturation indexes (ASI) lower than one, indicating a metaluminous character (not shown).

6.3. Trace element compositions of igneous and metasedimentary rocks

Generally, the mafic rocks have higher abundances in compatible trace elements (Ni. Cr, Sc), but lower concentrations of Ba, Rb, Cs and Th than tonalitic and granodioritic types (Fig. 7 and Table 1B). At equal SiO_2 contents, the diorites and tonalites interlayered within the mafic unit have slightly higher levels of compatible trace elements, but significantly lower Ba, Rb and Th than the tonalites and granodiorites that dominate the intermediate and silicic units (Fig. 7). In the gabbronoritic rocks, the concentration of compatible elements Ni and Cr is scattered. However, the abundances of Ni and Cr decrease at low SiO_2 contents, reflecting that Ni and Cr were incorporated into early crystallizing minerals. More important is that, excluding a few olivine or plagioclase cumulate rocks, the abundance of Cr and Ni in the mafic rocks is lower than that of primitive arc magmas (Fig. 7). Another distinctive characteristic is the somewhat smooth decrease of V and Sc with increasing SiO_2. Since V and Sc are incorporated into pyroxene, amphibole and magnetite with moderate to high partition coefficients (i.e. Kds = 1–5; Rollinson, 1993; Dunn and Sen, 1994; Nielsen et al., 1994) the behavior of these two metals shows that fractional crystallization of pyroxene, amphibole and/or oxides controlled in part the differentiation trend. There is no simple answer for observation that four mafic rocks fall outside the V *versus* SiO_2 trend. Unlike V and Sc, the variation of Co against SiO_2 cannot be accounted for by a unique petrologic process. The abundance of Sr displays an ill-defined trend with increasing SiO_2 and is strongly enriched in plagioclase-dominated cumulates. Furthermore, the concentration of Sr in non-cumulate mafic rocks is below the value expected for primitive arc magmas (Fig. 7). A common feature of strongly incompatible elements (shown by Rb and Th in Fig. 7) is that, at a given SiO_2 content, they are much more abundant in granodiorites than in tonalites. Whereas Ba shows an overall incompatible trend with increasing SiO_2, it does not follow the behavior of the other strongly incompatible elements (Rb and Th) which have clear compositional differences among the distinct igneous rock units.

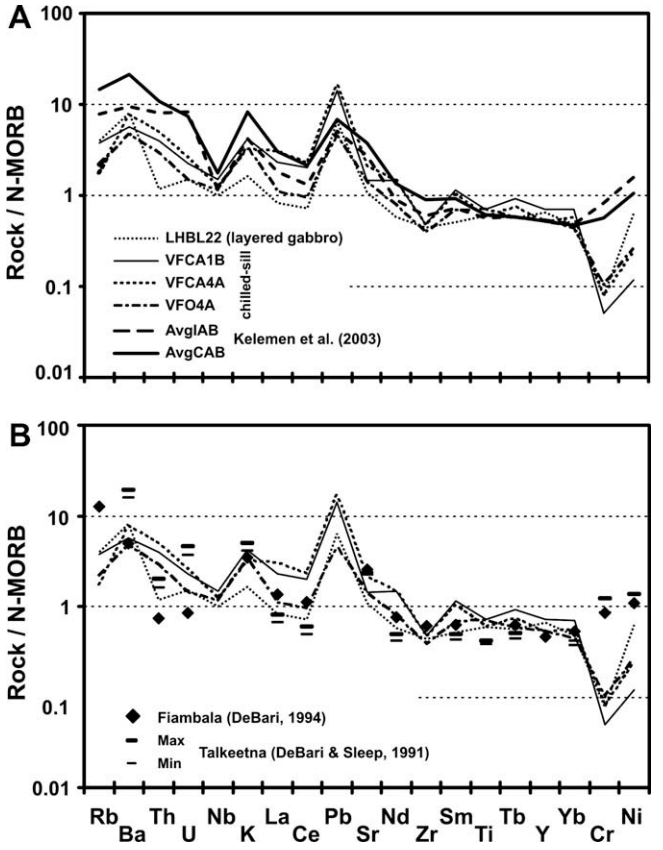

Fig. 10. Trace element composition of rocks considered to be the best candidate to represent the parental magma for the Valle Fértil-La Huerta paleo-arc section normalized to N-MORB values from Hofmann (1988). (A) Compares the studied mafic rocks with the trace element contents of primitive continental and island arc basalts from Kelemen et al. (2003). (B) Includes trace element patterns of parental magmas from paleo-arc lower crustal sections exposed in Talkeetna-Tonsina section DeBari and Sleep (1991) and Fiambalá gabbronoritic massif (e.g. DeBari (1994)).

The distinction among lithologic rock units is also observed from contrasting rare earth elements abundances shown in chondrite-normalized (REE_N) patterns (Fig. 8A–F). Gabbronoritic samples (SiO_2 <50 wt.%) display a broad band of REE_N profiles that change as the total amount of rare earth elements (∑REE) increases (Fig. 8A). Hence, with increasing ∑REE contents, the pattern varies from non-fractionated ($La_N/Yb_N = 1.2$) to slightly fractionated with $La_N/Yb_N < 4.4$, and from patterns showing the absence of Eu-anomaly ($=Eu_N/Eu^*_N$, where $Eu^*_N = \sqrt{Sm_N \cdot Gd_N}$) to patterns having a negative Eu-anomaly ($Eu_N/Eu^*_N \leqslant 0.6$). It should, however, be noted that the amphibole + pyroxene ± olivine cumulate rocks (VFJA7 and LHBL20) and the plagioclase-dominated rock (VFO3) are not expected to follow the trend of REE variation described above (Fig. 8B).

Granodiorites have the highest ∑REE contents among all igneous rocks (Fig. 8F). They also have well-fractionated REE patterns ($La_N/Yb_N = 5.5–6.9$) with most of the fractionation accommodated by LREE (La_N/Sm_N *ca.* 3.5) and negative Eu-anomalies of around 0.6. Importantly, the granodiorites have low Gd_N/Yb_N ratios (1.55–1.75) and flat heavy (HREE) rare earth element profiles at 15–24 times chondritic concentration, reflecting that garnet was not involved in the origin of the granodioritic magmas.

Tonalites from the intermediate unit and their microdioritic enclaves have strong light to heavy REE fractionated patterns ($La_N/Yb_N = 4.6–6.5$). In addition, some tonalites having low ∑REE show a weak concave upward pattern from MREE to HREE. The total abundance of REE (=∑REE) of tonalites is usually higher than those of mafic rocks but always lower than those of granodiorites. Furthermore, tonalites from the intermediate unit tend to have more REE than diorite and tonalites interlayered within the mafic unit (Fig. 8D and E).

7. Discussion

7.1. Parental magma composition for the paleo-arc crustal section from Valle Fértil-La Huerta

An objective of this study is to unravel the composition of the less evolved magmas that emplaced at the lower levels of the Famatinian paleo-arc. To our current understanding of the stratigraphic sequence, the deepest levels of this paleo-crust do not expose the lithospheric mantle–crust boundary. Thus, it is not possible to identify the magmas that fluxed out from the mantle and crossed the Mohorovicic discontinuity. The less-evolved mafic unit is lithologically complex and includes a wide variety of rocks, indicating that the composition of magmas feeding this unit changed while the arc crust was forming. Within this context, there are several reasons for pointing out that the chilled mafic sill/dike suite repre-

Table 2
Mass balance modeling through least square multiple regressions.

	Tonalite GVF14	Amph	Pl An66	Mt	Diorite VFO1A	Calc. VFO1A	r^2
Model 1 - crystal fractionation for the derivation of tonalite GVF14 from diorite VFO1A							
SiO_2	62.39	44.15	51.61	0.08	55.54	55.57	0.00
TiO_2	0.77	1.35		0.15	0.95	0.74	0.04
Al_2O_3	17.11	12.25	31.05	0.16	18.18	17.97	0.04
FeO^*	6.19	12.22	0.07	99.40	8.60	8.60	0.00
MnO	0.13	0.58		0.03	0.15	0.19	0.00
MgO	2.27	15.25		0.05	4.34	4.22	0.02
CaO	6.14	11.61	13.58	0.08	7.90	8.16	0.07
Na_2O	2.98	1.56	3.75		2.34	2.76	0.18
K_2O	1.78	1.03	0.10		1.76	1.32	0.19
P_2O_5	0.23				0.25	0.15	0.01
Coefficient	0.629	0.183	0.160	0.025		$\sum r^2$	0.56

	Granodiorite GVF10	Amph	Pl An53	Tonalite GVF14	Calc. GVF14	r^2
Model 3 - crystal fractionation for the derivation of granodiorite GVF10 from tonalite GVF14						
SiO_2	65.12	44.15	54.40	62.39	62.47	0.01
TiO_2	0.71	1.35		0.77	0.70	0.01
Al_2O_3	16.16	12.25	29.20	17.11	16.91	0.04
FeO^*	5.36	12.22	0.07	6.19	5.43	0.58
MnO	0.12	0.58		0.13	0.15	0.00
MgO	1.87	15.25		2.27	2.72	0.21
CaO	5.27	11.61	10.92	6.14	6.21	0.00
Na_2O	2.98	1.56	5.25	2.98	3.05	0.00
K_2O	2.21	1.03	0.14	1.78	1.95	0.03
P_2O_5	0.19			0.23	0.16	0.00
Coefficient	0.838	0.076	0.083		$\sum r^2$	0.88

	Diorite VFO6	Migma VFO11	Diorite VFO1A	Calc. VFO1A	r^2	Tonalite GVF14	Crustal Avg.	Granodio GVF10	Calc. GVF10	r^2
Model 2 - mixing diorite VFO6 and migmatites VFO11 for derivation of diorite VFO1A						*Model 4 - mixing tonalite and average supracrustal component for derivation of granodiorite GVF10*				
SiO_2	53.13	65.08	55.54	55.54	0.00	62.39	70.68	65.12	65.03	0.01
TiO_2	1.21	1.26	0.95	1.23	0.08	0.77	0.75	0.71	0.77	0.00
Al_2O_3	18.54	16.00	18.18	18.35	0.03	17.11	14.51	16.16	16.47	0.09
FeO^*	10.52	7.91	8.60	10.24	2.68	6.19	4.85	5.36	5.85	0.24
MnO	0.20	0.22	0.15	0.20	0.00	0.13	0.10	0.12	0.12	0.00
MgO	4.37	3.34	4.34	4.26	0.01	2.27	2.26	1.87	2.28	0.17
CaO	8.99	1.40	7.90	7.93	0.00	6.14	1.45	5.27	4.86	0.17
Na_2O	2.23	2.12	2.34	2.24	0.01	2.98	1.96	2.98	2.71	0.07
K_2O	0.54	2.59	1.76	0.86	0.81	1.78	3.37	2.21	2.23	0.00
P_2O_5	0.27	0.08	0.25	0.24	0.00	0.23	0.07	0.19	0.19	0.00
Coefficient	0.857	0.153		$\sum r^2$	3.62	0.725	0.280		$\sum r^2$	0.75

FeO^* is total Fe as FeO; $\sum r^2$ = is sum of square of the residuals.

Please cite this article in press as: Otamendi, J.E. et al., Geology and petrology of a deep crustal zone from the Famatinian paleo-arc, Sierras ..., J. S. Am. Earth Sci. (2009), doi:10.1016/j.jsames.2008.11.007

sents at least one of the magmas that fed the mafic unit. The more convincing arguments are: (1) the swarm of tabular-shaped intrusions is widespread through the mafic unit on a regional scale; (2) these intrusions have textures indicative of being frozen igneous liquids; and (3) the chilled mafic suite shows trace element signature generally resembling those characterizing primitive arc magmas. Another candidate is a two-pyroxene gabbroic rock (LHBL22) taken from a layered mafic body in the Sierra La Huerta. This gabbro has two attributes: (1) non-cumulate igneous texture with plagioclase + clinopyroxene + orthopyroxene + oxide assemblage, and (2) moderately high Mg-number (*ca.* 0.57). However, the major element composition of these mafic rocks differs from typical parental arc magmas in having relatively low Mg-number (<0.60) at low SiO_2 contents (Fig. 9A and B). Thus, the most primitive mafic rocks have not crystallized from magmas having been in equilibrium with a mantle peridotitic source (see Wilson, 1989). Furthermore, these mafic rocks have compositional characteristics of high-Al_2O_3 basalts (e.g. Crawford et al., 1987) because at the SiO_2 contents of primitive magmas (48–52 wt.%) their chemical trend is enriched in Al_2O_3 (>17 wt.%) and CaO (>8 wt.%). Major element composition suggests that differentiation started at deeper depths than those exposed in the lower Famatinian paleo-arc crust. Experimental results (e.g. Müntener et al., 2001) showed that at high pressure (>10 kbar) early differentiation of primitive hydrous basaltic melts is controlled by clinopyroxene and orthopyroxene (Fig. 9). The formation of dominantly pyroxenitic cumulate rocks (or residual rocks) after crystallization of hydrous basaltic melts (or water-fluxed partial melting of a basaltic source) produces derivative liquids which at high melt fractions have lower SiO_2 and Mg/Fe ratios but higher Al_2O_3 contents than their parental magma or source (Fig. 9C and D).

The mafic end-members of the Valle Fértil-La Huerta sequence can be derived from typical primary arc magmas, as sub-crustal differentiation trends of the primary magmas involve the extraction of Al_2O_3-poor and also expectedly MgO-rich early crystallizing mineral assemblages (e.g. Perfit et al., 1980; Gust and Perfit, 1987;

Table 3
Mineral/melt partition coefficients used in fractional crystallization and AFC models.

	Pl	Amph	Mt
Rb	0.01–0.06 (1)	0.29 (2)	0.001 (a)
Ba	0.38–1.45 (1)	0.42 (2)	0.001 (a)
Sr	1.4–3.5 (1)	0.46 (2)	0.001 (a)
K	0.17 (2)	0.96 (2)	0.001 (a)
Th	0.01–0.02 (1)	0.50 (2)	0.1 (2)
La	0.08–0.18 (1)	0.12–0.37 (3)	0.003 (4)
Sm	0.02–0.08 (1)	1.37–2.01 (3)	0.007 (4)
Eu	0.48–0.79 (1)	1.08–1.62 (3)	0.01 (a)
Gd	0.02–0.07 (1)	1.49–2.30 (3)	0.006 (4)
Yb	0.01 (1)	1.15–2.10 (3)	0.01 (a)

Data sources are: (1) Dunn and Sen (1994), (2) Rollinson (1993), (3) Klein et al. (1997), (4) Nielsen et al. (1994), and (a) assumed value.

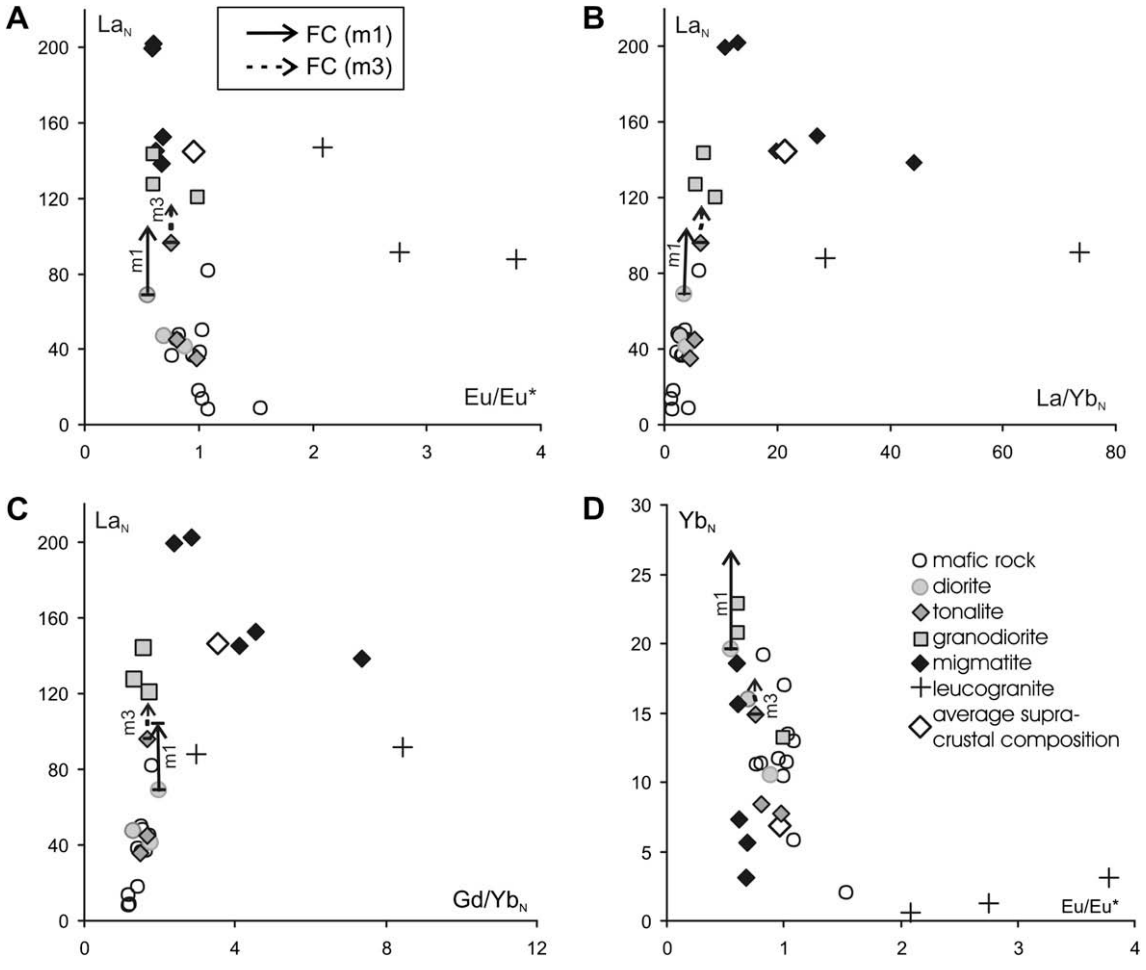

Fig. 11. (A–D). Results obtained after modeling closed-system fractional crystallization (m1 and m3 from Table 2) for rare earth elements. The concentrations of selected REE's are presented in chondrite-normalized abundances. The fractionating assemblages for fractional crystallization are those deduced from mass balance calculations (see Table 2) and partition coefficients are presented in Table 3.

Please cite this article in press as: Otamendi, J.E. et al., Geology and petrology of a deep crustal zone from the Famatinian paleo-arc, Sierras ..., J. S. Am. Earth Sci. (2009), doi:10.1016/j.jsames.2008.11.007

Pichavant and Macdonald, 2007). The idea that primary arc magmas experience differentiation beneath the arc crust is not new. The process of fractional crystallization and cumulate formation was observed in the Talkeetna-Tonsina arc section (DeBari and Sleep, 1991; Greene et al., 2006) and was inferred to occur in the roots of Cordilleran plutonic belts (Gromet and Silver, 1987; Ducea and Saleeby, 1996; Lee et al., 2006).

In spite of having major element contents different from those of primary arc magmas, the less-evolved mafic rocks have trace element signature with features interpreted to be characteristic of subduction-related primitive igneous rocks. The mafic rocks are characterized by enrichments in LILE and depletions in HFSE relative to the Normal-MORB's composition (Fig. 10). The multi-element patterns normalized to MORB show enrichments in lithophile incompatible elements, positive Pb anomaly, Nb depletion, and overall decreasing of abundance with increasing mantle compatibility. Hence, the trace element patterns are similar to those of typical plutonic and volcanic rocks in arc settings (Wilson, 1989). Notably, the only difference with typical arc primitive rocks is that the studied primitive mafic rocks appear strongly depleted in Cr and to a lesser extent in Ni. This is thereby consistent with what was deduced above because the depletion of Cr and Ni, which behave as strongly compatible trace elements, might be interpreted to be another effect of pyroxenes ± olivine crystallization at non-exposed sub-crustal levels. Ni/Cr ratio of studied mafic rocks (>0.5) is higher than those of primitive arc magmas (normally <0.45), reflecting that Cr is more depleted than Ni. This Ni/Cr ratio requires removal of more pyroxene than olivine, even though the alternative cannot be ruled out that Cr was incorporated into chromite and/or Cr-rich spinel. Furthermore, compared to normal primitive arc magmas the mafic rocks are depleted in Ni, reflecting that olivine was also involved during the initial stage of magmatic differentiation.

7.2. Mass balance constraints on petrologic processes

Mass balance through least squares multiple-regressions is used to test petrologic processes potentially linking lithologies from the different rock units. Mass balance models combined whole-rock major element chemistry with measured mineral compositions (Table 2). Models using gabbronorites and some low-K_2O diorites as starting compositions fail to reproduce typical tonalities. This is because the K_2O content (<0.6 wt.%) of the low-K_2O diorites is too low to derive a typical tonalite containing K_2O >1.7 wt.%. In contrast, using a high-K_2O diorite (VFO1A) as starting parental rocks, subtraction of 18 wt.% amphibole, 16 wt.% plagioclase (An_{66}) and 2.5% magnetite produces a composition closely resembling a typical tonalite (model 1 in Table 2, where goodness of fit is measured by $\sum R^2 = 0.56$). The problem immediately arises why there are distinct diorites. In this regards, mass balance shows that mixing a typical migmatite (VFO11) with a low-K_2O diorite (VFO6) reproduces the composition of the high-K_2O diorites (VFO1A). This model shown as model 3 in Table 2 does not fit well ($\sum R^2 = 3.62$); however, most of its divergence (75%) is due to FeO^*. This result is consistent with field relations as low-K_2O and high-K_2O diorites are interlayered with migmatites within the mafic unit. Thus, the difference between low-K_2O and high-K_2O diorites might be one of the amounts of metasedimentary migmatite incorporated into the dioritic magmas.

Successful mass balance modeling shows that there exist two alternatives for deriving a typical granodiorite (GVF10) starting from tonalite (GVF14). Furthermore, each alternative validated through mass balance models entails distinct petrologic processes (see models 2 and 4 in Table 2). In one model, granodiorite (GVF10) is derived from tonalite (GVF14) by extracting similar amounts (*ca.* 8 wt.%) of plagioclase (An_{53}) and amphibole. This model passes the petrologic test, for the abundance and composition of fractionating phases roughly match those found in tonalities. Alternatively, mixing 28 wt.% of an average supracrustal composition (computed using whole rock composition of five migmatites and three leucogranites, see Table 1) with 72 wt.% of a typical tonalite (GVF14) improves the fit of the calculated granodiorite composition. It might be argued that mass balance is not conclusive about which process has more relevance in moving the differentiation trend from tonalites to granodiorites. Thus, the petrologic processes will be further evaluated using trace element systematics because trace element's trends provide clearer and additional proofs. It should be noted that trace element modeling is tenable only if mass balance results are used as constraints.

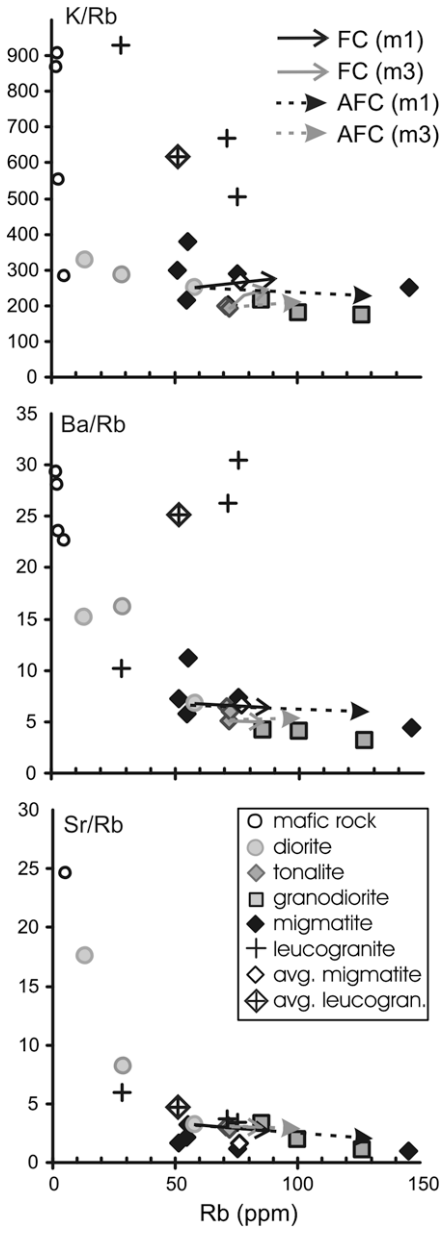

Fig. 12. Simple fractional crystallization (FC) and assimilation fractional crystallization (AFC) models for large ion lithophile elements. The fractionating phase assemblages are those computed through mass balance; m1 is for model 1, m3 is for model 3 (see Table 2). The trace element abundances of the parental magmas are also those corresponding to the starting compositions in mass balance models (e.g. VFO1A and GVF14, respectively), and the composition of the assimilant is the average of the paragneissic migmatites and anatectic leucogranites.

Please cite this article in press as: Otamendi, J.E. et al., Geology and petrology of a deep crustal zone from the Famatinian paleo-arc, Sierras ..., J. S. Am. Earth Sci. (2009), doi:10.1016/j.jsames.2008.11.007

7.3. Origin of intermediate and silicic rocks constrained through trace element modeling

The idea that intermediate and silicic plutonic rocks are largely derived by fractional crystallization (or partial melting) of less evolved magmas (or magmatic rock) is supported by the fact that tonalites and granodiorites contain the lowest contents of strongly compatible elements (Ni and Cr, see Fig. 7). This feature places limits to the amount of paragneissic migmatites assimilated into the igneous magmas, as the migmatites have higher Ni and Cr abundances than the tonalites and granodiorites. By contrast, owing to the tonalites, granodiorites and anatectic leucogranites all have similar Cr and Ni contents, the feasibility that mixing of dioritic magmas and leucogranites has generated tonalitic and/or granodioritic magmas is not easy to be tested using strongly compatible elements.

Fractional crystallization is also supported by the variation of the rare earth elements. The REE modeling uses the mineral/melt partition coefficients shown in Table 3 and the proportions of crystallizing mineral phases estimated in the mass balance calculations (Table 2). As illustrated in Fig. 11A–D, Rayleigh fractionation modeling replicates the overall increment of LREE (La_N) with little changes in Eu/Eu^*, the rather constant fractionation between LREE and HREE (La_N/Yb_N), and the absence of differentiation from MREE to HREE (Gd_N/Yb_N). However, models cannot replicate the concentrations of HREE (measured as Yb_N) because HREE abundances do not show a defined differentiation trend among the igneous rocks (Fig. 11D). Furthermore, in order to reproduce the concentration of LREE (La_N) found in some granodiorites, the modeling of REE would require using higher degrees of fractional crystallization ($F > 0.6$) than those supported by mass balance models (Fig. 11A–C).

Fractional crystallization modeling of LIL elements also indicates that the high-K_2O diorites can serve as parental magmas for the typical tonalites, whereas the granodiorites can be derived from the parental tonalitic magmas (Fig. 12). This result is consistent with mass balance calculations, which estimate that about 37% crystallization of a high-K_2O diorite (VFO1A in Table 1) would form a typical tonalite (GVF14), and 16% crystallization in the tonalitic magma is sufficient to produce the granodiorite (e.g. GVF10). However, these degrees of fractional crystallization are insufficient to replicate the concentration of incompatible trace elements in some granodiorites (Figs. 12 and 13). The concentration of the strongly incompatible trace element (Rb, Th and La) in the tonalites and granodiorites seems to be too high to result from closed-system fractional crystallization from the mafic gabbronorites and low-K_2O diorites. Rayleigh fractionation models using the low-K_2O diorites as parental composition produce derivative liquids that have Rb, La, Th, and K abundances that are at least 1.5 times lower than the abundances in the granodiorites. This is illustrated by the failure of the models to reproduce the abundance of Rb, La and Th, which have similar and low bulk partition coefficients ($D_{Rb} < 0.06$, $D_{Th} < 0.10$ and $D_{La} < 0.12$). These preceding arguments suggest that at some step(s) of the igneous evolutionary sequence there is an input of mass derived from a supracrustal component.

Field relationships suggest that the incorporation of the supracrustal rocks can be accomplished in two forms. The paragneissic migmatites might be bulk assimilated, whereas the anatectic leucogranites segregated from the migmatites could mix with the igneous magmas.

The model conventionally utilized to test open-system petrologic processes involves wall-rock assimilation concurrent with

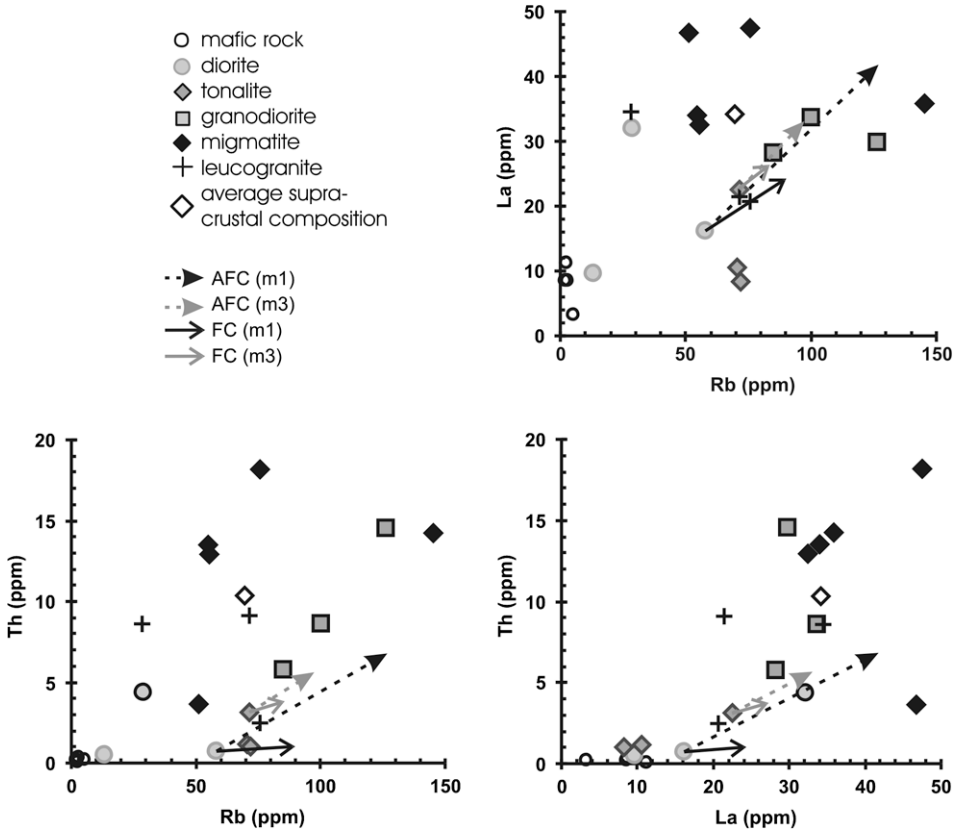

Fig. 13. Simple fractional crystallization (FC) and assimilation fractional crystallization (AFC) models for the most incompatible elements. Models were computed using the same data as those described in Fig. 12. In this particular case, the results of models are largely independent of mineral assemblage and partition coefficients because of the strongly incompatible nature ($D < 0.1$) of the modeled elements. From these models it is shown that some granodiorites are not easily generated from less evolved dioritic or tonalitic magmas through closed-system fractional crystallization. Furthermore, the incapacity of generating granodiorites would be more marked if less evolved rock (e.g. gabbronorite or low-K_2O diorite) were used as starting compositions.

Please cite this article in press as: Otamendi, J.E. et al., Geology and petrology of a deep crustal zone from the Famatinian paleo-arc, Sierras ..., J. S. Am. Earth Sci. (2009), doi:10.1016/j.jsames.2008.11.007

fractional crystallization (AFC). This process is here modeled with the equations of DePaolo (1981). The models use an average supracrustal composition for the assimilant, and the fractionating mineral phases determined in the mass balance (i.e. models 1 and 3 in Table 2). The assimilant composition was obtained by averaging five paragneissic migmatites and three leucogranites (see Table 1). A conservative "*r*" ratio of 0.5 is assumed for modeling AFC processes (see DePaolo, 1981). As a general result, AFC modeling improves the results obtained with closed-system crystallization. AFC models of the most incompatible elements match the Rb and La compositions of the evolved granodiorites, but Th abundances are not well reproduced (Fig. 13). The distinct behavior of trace elements provides strong evidence for decoupling of the processes responsible for producing variable elemental abundances. The strongly compatible trace elements are to a large extent governed by fractional crystallization, for example Ni and Cr concentrations are depleted at an early stage of the igneous evolutionary sequence and as a result of closed-system fractional crystallization. In contrast, the strongly incompatible elements that are highly enriched in the more evolved intermediate and silicic rocks reflect the effects of an open-system process involving igneous magmas and supracrustal rocks.

8. Conclusions

Field observations, petrographic analyses, mineral compositions and whole-rock chemical data indicate that a mafic primitive melt fed the less-evolved mafic unit and fluxed into the entire arc crust section. The non-cumulate mafic rocks have somewhat low Mg-number and high Al_2O_3 composition compared to the primary magmas of oceanic and continental magmatic arcs. This difference suggests fractionation of mantle-derived magmas at deeper levels than those exposed in the paleo-arc Famatinian crust. Differentiation of mafic parental magmas generates a wide variety of amphibole-bearing and/or plagioclase-rich gabbronorites; even higher degrees of fractionation produce amphibole diorites with variable amounts of orthopyroxene and sporadic biotite. Mass balance calculations show that a (supra)crustal metasedimentary input better accounts for the major element composition of high-K_2O diorites interlayered with igneous mafic rocks. An important conclusion is to recognize the existence of subalkaline intermediate magmas having low-K_2O and normal-K_2O signatures, because the difference in K_2O contents might be one of the amount of metasedimentary material incorporated into evolving igneous magmas. In terms of both major element mass balance and trace element systematics typical tonalitic magmas can result from closed-system differentiation of a parental dioritic magma. Furthermore, the typical tonalites cannot be derived from primitive gabbronoritic parent. The change from tonalite-dominated unit to granodiorite-dominated unit spreads over a wide belt characterized by mingling of tonalitic and leucogranitic magmas, which are together intruded by mafic dikes. The continuous variation in mineral modal proportion (excluding the steady increment of K-feldspar) and of whole-rock chemical features implies that amphibole biotite granodiorites are cogenetic with tonalites. Since the majority of preceding studies regarded Sierras Valle Fértil-La Huerta as a complex metamorphic basement separated in sharp contact from a granodioritic batholith, this work provides the view that the geological section exposed along these sierras is altogether a single paleo-arc crust and as a whole the plutonic rock sequence is genetically related.

Acknowledgements

Critical reviews by Suzanne Kay and two anonymous referees are thanked. We specially acknowledge Dra. Kay who provides some thousand hints on writing style. We thank George Bergantz for his contributing discussions and reading the manuscript. This work was funded by ANPCYT-Argentina PICTR Grant no. 20298/04, CONICET Grant no. PIP 5211, and by a complementary Grant from SeCyT-UNRC. The senior author thanks University of Huelva, Spain, for supporting him through a visiting professor contract that enabled his accessing the microprobe facilities.

Appendix A. Supplementary material

Supplementary data associated with this article can be found, in the online version, at doi:10.1016/j.jsames.2008.11.007.

References

Aceñolaza, F.G., Miller, H., Toselli, A.J., 2000. The Pampean and Famatinian cycles – superposed orogenic events in the West Gondwana. Sonderheft ZAG SH1, 337–344.

Anders, E., Grevesse, N., 1989. Abundances of the elements-meteoritic and solar. Geochimica et Cosmochimica Acta 53, 197–214.

Arculus, R.J., Wills, K.J.A., 1980. The petrology of plutonic blocks and inclusions from the Lesser Antilles Island Arc. Journal of Petrology 21, 743–799.

Astini, R.A., Dávila, F.M., 2004. Ordovician back arc foreland and Ocloyic thrust belt development on the western Gondwana margin as a response to Precodillera terrane accretion. Tectonics 23, TC4008. doi:10.1029/2003TC001620.

Baldo, E.J., Murra, J., Casquet, C., Saavedra, J., Galindo, C., 1999. Gabros coroníticos de la Sierra de Valle Fértil. Química mineral y condiciones P-T. Sierras Pampeanas occidentales (Argentina). Boletín de la Sociedad Española de Mineralogía 22A, 17–19.

Beard, J.S., 1986. Characteristic mineralogy of arc-related cumulate gabbros: implications for the tectonic setting of gabbroic plutons and for andesite genesis. Geology 14, 848–851.

Büttner, S.H., Glodny, J., Lucassen, F., Wemmer, K., Erdmann, S., Handler, R., Franz, G., 2005. Ordovician metamorphism and plutonism in the Sierra de Quilmes metamorphic complex: implications for the tectonic setting of the northern Sierras Pampeanas (NW Argentina). Lithos 83, 143–181.

Caminos, R., 1979. Sierras Pampeanas noroccidentales. Salta, Tucumán, Catamarca, La Rioja y San Juan. In: Leanza, E.F. (Ed.), II Simposio de Geología Regional Argentina. Academia Nacional de Ciencias de Córdoba, pp. 225–291.

Castro, A., Martino, R., Vujovich, G., Otamendi, J., Pinotti, L., D'eramo, F., Tibaldi, A., Viñao, A., 2008. Top–down structures of mafic enclaves within the Valle Fértil magmatic complex, San Juan, Argentina. Geologica Acta 6, 217–229.

Castro de Machuca, B., Arancibia, G., Morata, D., Belmar, M., Previley, L., Pontoriero, S., 2008. P-T-t evolution of an Early Silurian medium-grade shear zone on the west side of the Famatinian magmatic arc, Argentina: implications for the assembly of the Western Gondwana margin. Gondwana Research 13, 216–226.

Cisterna, C.E., 2001. Volcanismo subácueo en el Eopaleozoico del Sistema de Famatina, noroeste de Argentina. Revista de la Asociación Geológica Argentina 56, 16–24.

Coira, B., Pérez, B., Flores, P., Kay, S.M., Woll, B., Hanning, M., 1999. Magmatic sources and tectonic setting of Gondwana margin Ordovician magmas, northern Puna of Argentina and Chile. In: Ramos, V., Keppie, J. (Eds.), Laurentia-Gondwana Connections Before Pangea, vol. 336. Geological Society of America, pp. 145–170. Special paper.

Crawford, A.J., Falloon, T.J., Eggins, S., 1987. The origin of island arc high-alumina basalts. Contributions to Mineralogy and Petrology 97, 417–430.

de Alba, E., 1979. Sistema de Famatina. In: Leanza, E.F. (Ed.), II Simposio de Geología Regional Argentina. Academia Nacional de Ciencias de Córdoba, pp. 349–395.

DeBari, S., 1994. Petrogenesis of the Fiambalá gabbroic intrusion, Northwestern Argentina, a deep crustal syntectonic pluton in a continental magmatic arc. Journal of Petrology 35, 679–713.

DeBari, S., Coleman, R.G., 1989. Examination of the deep levels of an island arc: evidence from the Tonsina ultramafic-mafic assemblage, Tonsina, Alaska. Journal of Geophysical Research 94, 4373–4391.

DeBari, S., Sleep, N.H., 1991. High-Mg, low-Al bulk composition of the Talkeetna island arc, Alaska: implications for primary magmas and the nature of arc crust. Geological Society of America Bulletin 103, 37–47.

de la Rosa, J.D., Chacón, H., Sánchez-de-la-Campa, A., Carrasco, R., Nieto, J.M., 2001. Metodología y análisis de elementos trazas-REE mediante ICP-MS del standard SARM 1 (granito) y SARM 4 (norita). In: Lago, M., Arranz, E., Galé, C. (Eds.), Libro de Actas del III Congreso Ibérico de Geoquímica. Zaragoza, España, pp. 435–438.

DePaolo, D.J., 1981. A neodymium and strontium isotopic study of the Mesozoic calc-aklaline granitic batholiths of the Sierra Nevada and Peninsular Ranges, California. Journal of Geophysical Research 86, 10470–10488.

Ducea, M.N., Kidder, S., Zandt, G., 2003. Arc composition at mid-crustal depths: insights from the Coast Ridge Belt, Santa Lucia Mountains, California. Geophysical Research Letters 30, 1703. doi:10.1029/2002GL016297.

Ducea, M.N., Saleeby, J.B., 1996. Buoyancy sources for a large, unrooted mountain range, the Sierra Nevada, California: evidence from xenolith thermobarometry. Journal of Geophysical Research 101, 8226–8244.

Dungan, M.A., Wulff, A., Thompson, R., 2001. Eruptive stratigraphy of the Tatara-San Pedro Complex 36 S, southern volcanic zone, Chilean Andes: reconstruction method and implications for magma evolution at long-lived arc volcanic centers. Journal of Petrology 42, 555–626.

Dunn, T., Sen, C., 1994. Mineral/matrix partition coefficients for orthopyroxene, plagioclase, and olivine in basaltic to andesitic systems: a combined analytical and experimental study. Geochimica et Cosmochimica Acta 58, 717–733.

Fanning, C.M., Pankhurst, R.J., Rapela, C.W., Baldo, E.G., Casquet, C., Galindo, C., 2004. K-bentonites in the Argentine Precodillera contemporaneous with rhyolite volcanism in the Famatinian arc. Journal of the Geological Society, London 161, 747–756.

Feeley, T.C., Dungan, M.A., Frey, F.A., 1996. Geochemical constraints on the origin of mafic and silicic magmas at Cordón El Guadal, Tatara-San Pedro Complex, central Chile. Contributions to Mineralogy and Petrology 131, 393–411.

Gamble, J.A., Wood, C.P., Price, R.C., Smith, I.E.M., Stewart, R.B., Waight, T., 1999. A fifty year history of magmatic evolution on Ruapehu Volcano, New Zealand: verification of open system behaviour in an arc volcano. Earth and Planetary Science Letters 170, 301–314.

García-Moreno, O., Castro, A., Corretgé, L.G., El-Hmidi, H., 2006. Dissolution of tonalitic enclaves in ascending hydrous granitic magmas: an experimental study. Lithos 89, 245–258.

Garrido, C.J., Bodinier, J.-L., Burg, J.-P., Zilinger, G., Hussain, S.S., Dawood, H., Chaudhry, M.N., Gervilla, F., 2006. Petrogenesis of mafic garnet granulite in the lower crust of the Kohistan paleo-arc complex (Northern Pakistan): implications for intra-crustal differentiation of island arcs and generation of continental crust. Journal of Petrology 47, 1873–1914.

Giménez, M.E., Martínez, M.P., Introcaso, A., 2000. A crustal model based mainly on gravity data in the area between the Bermejo Basin and the Sierras de Valle Fértil, Argentina. Journal of South America Earth Sciences 13, 275–286.

Greene, A.R., DeBari, S., Kelemen, P.B., Blusztajn, J., Clift, P., 2006. A detailed geochemical study of island arc crust: the Talkeetna arc section, south–central Alaska. Journal of Petrology 47, 1051–1093.

Gromet, P., Silver, L.T., 1987. REE variations across the peninsular ranges Batholith: implications for batholith petrogenesis and crustal growth in magmatic arcs. Journal of Petrology 28, 75–125.

Grove, T.L., Kinzler, R.J., 1986. Petrogenesis of andesites. Annual Review of Earth and Planetary Sciences 14, 417–454.

Gust, D.A., Perfit, M.R., 1987. Phase relations of a high-Mg basalt from the Aleutian island arc: implications for primary island arc basalts and high-Al basalts. Contributions to Mineralogy and Petrology 97, 7–18.

Hofmann, A.W., 1988. Chemical differentiation of the earth: relationship between mantle, continental crust and oceanic crust. Earth and Planetary Science Letters 90, 297–314.

Jordan, T.E., Allmendinger, R.W., 1986. The Sierras Pampeanas of Argentina: a modern analogue of rocky mountain foreland deformation. American Journal of Science 286, 737–764.

Kelemen, P.B., Hanghøj, K., Greene, A.R., 2003. One view of the geochemistry of subduction-related magmatic arcs, with emphasis on primitive andesite and lower crust. In: Rudnick, R. (Ed.), The Crust. In: Holland, H.D., Turekian, K.K. (Eds.), Treatise on Geochemistry, vol. 3. Elsevier-Pergamon, Oxford, pp. 596–659.

Kepleis, K.A., Clarke, G.L., Gehrels, G., Vervoort, J., 2004. Processes controlling vertical coupling and decoupling between the upper and lower crust of orogens: results from Fiorland, New Zealand. Journal of Structural Geology 26, 765–791.

Klein, M., Stosch, H.-G., Seck, H.A., 1997. Partitioning of high field-strength and rare-earth elements between amphibole and quartz-dioritic to tonalitic melts: an experimental study. Chemical Geology 138, 257–271.

Kretz, R., 1983. Symbols for rock-forming minerals. American Mineralogist 68, 277–279.

Leake, B., Woolley, A., Arps, C., Birch, W., Gilbert, M., Grice, J., Hawthorne, F., Kato, A., Kisch, H., Krivovichev, V., Linthout, K., Laird, J., Mandarino, J., Maresch, W., Nickel, E., Rock, N., Schumacher, J., Smith, D., Stephenson, N., Ungaretti, L., Whittaker, E., Youzhi, G., 1997. Nomenclature of amphiboles: report of the subcommittee on amphiboles of the international minerals and minerals names. American Mineralogist 82, 1019–1037.

Lee, C.-T.A., Cheng, X., Horodyskyj, U., 2006. The development and refinement of continental arcs by primary basaltic magmatism, garnet pyroxenite accumulation, basaltic recharge and delamination: insights from the Sierra Nevada, California. Contributions to Mineralogy and Petrology 151, 222–242.

Le Maitre, R.W., 1989. A classification of igneous rocks and glossary of terms. Blackwell, Oxford, 193 p.

Lucassen, F., Franz, G., 2005. The early palaeozoic orogen in the central Andes: a non-collisional orogen comparable to the cenozoic high plateau? In: Vaughan, A., Leat, P., Pankhurst, R. (Eds.), Terrane Processes at the Margins of Gondwana, vol. 246. Geological Society London, pp. 257–373. Special Publication.

Mannhein, R., Miller, H., 1996. Las rocas volcánicas y subvolcánicas eopaleozoicas del Sistema de Famatina. In: Aceñolaza, F.G., Miller, H., Toselli, A. (Eds.), Geología del Sistema de Famatina. Münchner Geologische Hefte A19. Münchnen. pp. 159–186.

Mirré, J.C., 1976. Descripción geológica de la Hoja 19e, Valle Fértil, provincias de San Juan y La Rioja. Servicio Geológico Nacional, Boletín No. 147, Buenos Aires. p. 70.

Miyashiro, A., 1974. Volcanic rock series in island arcs and active continental margins. American Journal of Sciences 274, 321–355.

Müntener, O., Kelemen, P.B., Grove, T.L., 2001. The role of H_2O during crystallization of primitive arc magmas under uppermost mantle conditions and genesis of igneous pyroxenites: an experimental study. Contributions to Mineralogy and Petrology 141, 643–658.

Murra, J., Baldo, E., 2006. El metamorfismo de las rocas básicas y ultrabásicas de la Sierra de La Huerta-Las Imanas (Sierras Pampeanas, Argentina): caracterización tectonotérmica del margen occidental del orógeno Famatiniano. Revista Geológica de Chile 33, 277–298.

Nicolas, A., 1992. Kinematics in magmatic rocks with special reference to gabbro. Journal of Petrology 33, 891–915.

Nielsen, R.L., Forsythe, L.M., Gallaghan, W.E., Fisk, M.R., 1994. Major and trace element magnetite-melt partitioning. Chemical Geology 117, 167–191.

Otamendi, J.E., Tibaldi, A.M., Vujovich, G.I., Viñao, G.A., 2008. Metamorphic evolution of migmatites from the deep Famatinian arc crust exposed in Sierras Valle Fértil-La Huerta, San Juan, Argentina. Journal of South American Earth Sciences 25, 313–335.

Pankhurst, R.J., Rapela, C.W., Saavedra, J., Baldo, E., Dahlquist, J., Pascua, I., Fanning, C.M., 1998. The Famatinian magmatic arc in the central Sierras Pampeanas: an early to mid-ordovician continental arc on the Gondwana margin. In: Pankhurst, R.J., Rapela, C.W. (Eds.), The Proto-Andean Margin of Gondwana, vol. 142. Geological Society London, pp. 343–368. Special Publication.

Pankhurst, R.J., Rapela, C.W., Fanning, C.M., 2000. Age and origin of coeval TTG, I- and S-type granites in the Famatinian belt of NW Argentina. Transactions of the Royal Society of Edinburgh: Earth Sciences 91, 151–168.

Perfit, M.R., Gust, D.A., Bence, A.E., Arculus, R.J., Taylor, S.R., 1980. Chemical characteristics of island arc basalts: implications for mantle sources. Chemical Geology 30, 227–256.

Pichavant, M., Macdonald, R., 2007. Crystallization of primitive basaltic magmas at crustal pressures and genesis of the calc-alkaline igneous suite: experimental evidence from St Vincent, Lesser Antilles arc. Contributions to Mineralogy and Petrology 154, 535–558.

Pontoriero, S., Castro de Machuca, B., 1999. Contribution to the age of the igneous-metamorphic basement of La Huerta range, province of San Juan, Argentina. In: Proceedings of the Second South American Symposium of Isotopic Geology. pp. 101–104.

Quenardelle, S., Ramos, V., 1999. The ordovician western Sierras Pampeanas magmatic belt: record of Argentine Precordillera accretion. In: Ramos, V.A., Keppie, D. (Eds.), Laurentia Gondwana Connections before Pangea, vol. 336. Geological Society of America, Boulder, pp. 63–86. Special Paper.

Ramos, V.A., 1995. Sudamérica: un mosaico de continentes y océanos. Ciencia Hoy 6, 24–29.

Ramos, V.A., Vujovich, G.I., Dallmeyer, R.D., 1996. Los klippes y ventanas tectónicas de la estructura preándica de la Sierra de Pie de Palo (San Juan): edad e implicanciones tectónicas. In: Proceedings of the Actas XIII Congreso Geológico Argentino y III Congreso de Exploración de Hidrocarburos, vol. 5. pp. 377–392.

Rapela, C.W., Coira, B., Toselli, A., Saavedra, J., 1992. The lower paleozoic magmatism of southwestern Gondwana and the evolution of Famatinian orogene. International Geology Review 34, 1142–10081.

Roeske, S., McClelland, W., Cain IV, J., Mulcahy, S., Vujovich, G., Iriondo, A., 2005. Paleozoic record of convergence and extension within the arc-forearc transition of the Famatinian arc, as recorded in western Sierra de la Huerta, Argentina. In: Pankhurst, R., Veiga, G. (Eds.), Gondwana 12: Abstracts. Academia Nacional de Ciencias, Córdoba, p. 315.

Rollinson, H.R., 1993. Using geochemical data: evaluation, presentation, interpretation. Longman Scientific and Technical, England, 352 p.

Rossi, J.N., Toselli, A.J., Saavedra, J., Sial, A.N., Pellitero, E., Ferreira, V.P., 2002. Common crustal source for contrasting peraluminous facies in the early paleozoic Capillitas Batholith, NW Argentina. Gondwana Research 5, 325–337.

Saavedra, J., Toselli, A., Rossi, J., Pellitero, E., Durand, F., 1998. The early palaeozoic magmatic record of Famatina system: a review. In: Pankhurst, R.J., Rapela, C.W. (Eds.), The Proto-Andean Margin of Gondwana, vol. 142. Geological Society London, pp. 283–295. Special Publication.

Sato, A.M., González, P.D., Llambías, E.J., 2003. Evolución del orógeno Famatiniano en la Sierra de San Luis: magmatismo de arco, deformación y metamorfismo de bajo a alto grado. Revista de la Aociación Geológica Argentina 58, 487–504.

Sisson, T.W., Grove, T.L., Coleman, D.S., 1996. Hornblende gabbro sill complex at Onion valley, California, and a mixing origin for the Sierra Nevada batholith. Contributions to Mineralogy and Petrology 126, 81–108.

Stair, K., Ducea, M., Otamendi, J.E., Gehrels, G., Bergantz, G., 2007. U-Pb zircon plutonic emplacement and metamorphic ages from a tilted crustal section of the Famatinian arc, northwestern Argentina: petrologic and regional tectonic implications. In: Proceeding of the Ores and Orogenesis: Circum-Pacific Tectonics, Geologic Evolution, and Ore Deposits, Tucson. p. 245.

Thomas, W.A., Astini, R.A., 1996. The Argentine precordillera: a traveler from the ouachita embayment of North American Laurentia. Science 273, 752–757.

Toselli, A.J., Durand, F.R., Rossi de Toselli, J.N., Saavedra, J., 1996. Esquema de evolución geotectónica y magmática Eopaleozoica del sistema de Famatina y sectores de Sierras Pampeanas. In: Proceedings of the Actas XIII Congreso Geológico Argentino y III Congreso de Exploración de Hidrocarburos, vol. 5. pp. 443–462.

Toselli, A.J., Saavedra, J., Pellitero, E., Rossi de Toselli, J.N., Aceñolaza, F.G., Medina, M.E., 1990. Geoquímica y petrogenesis del volcanismo Ordovícico de la formación Las Planchadas, Sistema de Famatina. Revista de la Asociación Geológica Argentina 45, 313–322.

Turner, J.C., Méndez, V., 1979. Puna. In: Leanza, E.F. (Ed.), Proceedings of the II Simposio de Geología Regional Argentina, Academia Nacional de Ciencias, Córdoba. pp. 117–142.

Please cite this article in press as: Otamendi, J.E. et al., Geology and petrology of a deep crustal zone from the Famatinian paleo-arc, Sierras ..., J. S. Am. Earth Sci. (2009), doi:10.1016/j.jsames.2008.11.007

Viramonte, J.M., Becchio, R.A., Viramonte, J.G., Pimentel, M.M., Martino, R.D., 2007. Ordovician igneous and metamorphic units in southeastern Puna: new U–Pb and Sm–Nd data and implications for the evolution of northwestern Argentina. Journal of South American Earth Sciences 24, 167–183.

Vujovich, G.I., Godeas, M., Marín, G., Pezzutti, N., 1996. El complejo magmático de la Sierra de La Huerta, provincia de San Juan. In: Proceedings of the Actas XIII Congreso Geológico Argentino y III Congreso de Exploración de Hidrocarburos, vol. 3. pp. 465–475.

Vujovich, G., Chernicoff, J., Tchiliguirian, P., Godeas, M., Marín, G., Pezzutti, N., Sepúlveda, E., 1998. Hoja geológica 3166-III, Chepes, provincias de San Juan y La Rioja. Subsecretaría de Minería de la Nación, Servicio Geológico Minero Argentino, Buenos Aires, 54 p.

Vujovich, G.I., Ramos, V.A., 1999. Mapa geotectónico de la República Argentina (1:2.500.000), Subsecretaría de Minería de la Nación, Buenos Aires, Servicio Geológico Minero Argentino.

Wiebe, R.A., Blair, K.D., Hawkins, D.P., Sabine, C.P., 2002. Mafic injections, in situ hybridization, and crystal accumulation in the Pyramid Peak granite, California. Bulletin of the Geological Society of America 114, 909–920.

Wilson, M., 1989. Igneous Petrogenesis. Chapman and Hall, London, 466 p.

Please cite this article in press as: Otamendi, J.E. et al., Geology and petrology of a deep crustal zone from the Famatinian paleo-arc, Sierras ..., J. S. Am. Earth Sci. (2009), doi:10.1016/j.jsames.2008.11.007